RESEARCH ARTICLE

Analysis of Wind Characteristics for Grid-Tied Wind Turbine Generator Using Incremental Generative Adversarial Network Model

RAMESH KUMAR BEHARA AND AKSHAY KUMAR SAHA[ID]**, (Senior Member, IEEE)**
Discipline of Electrical, Electronic, and Computer Engineering, University of KwaZulu-Natal, Durban 4041, South Africa

Corresponding author: Akshay Kumar Saha (saha@ukzn.ac.za)

ABSTRACT Wind attribute analysis is a crucial aspect of meteorological and environmental research, with applications ranging from renewable energy generation to weather forecasting. However, existing models encounter several challenges in accurately and comprehensively characterizing wind positions. In this context, the proposed Incremental Tuned Generative Adversarial Network model (incremental GAN model), based on an unsupervised learning approach, introduces innovative solutions to overcome these challenges and enhance the precision and reliability of wind position analysis. This research aims to enhance the reliability and efficiency of wind energy generation by analyzing wind conditions and providing accurate data for decision-making. It introduces an Incremental GAN that refines parameters based on various factors. This GAN model learns and predicts these parameters over time, improving its performance. It incorporates advanced techniques like a 2-level fused discriminator and self-attention for precise predictions of wind characteristics. The GAN model generates important parameters such as droop gain, which influences generator output in response to load or generation changes, aiding grid stability. It also optimizes the frequency control of different types of generators in the presence of wind farms. The model continuously monitors wind farm conditions, adjusting power injection into the grid as needed for efficient and reliable wind energy utilization.

INDEX TERMS Renewable energy system (RES), wind energy integration (WEI), power system stability (PSS), unsupervised learning (USL), incremental tuned generative adversarial network (IGAN), doubly fed induction generator (DFIG), synchronous generator (SG).

I. INTRODUCTION

Renewable energy sources (RES) are becoming increasingly crucial in meeting the world's future energy requirements. They are gradually replacing conventional energy sources, thereby mitigating the risks associated with the widespread use of traditional energy sources [1]. With growing concerns about climate change, the imperative to generate clean and eco-friendly power has never been more pressing [2]. The intensive consumption of electrical energy, coupled with escalating hydrocarbon prices and a heightened environmental consciousness, has prompted numerous nations to launch

both national and international initiatives aimed at harnessing electricity from renewable resources [3], [4]. However, renewable energy sources possess a distinctive characteristic that they are often unpredictable and intermittent. This unpredictability can lead to significant challenges concerning the stability of electricity grids [5], [6]. Wind energy, one of the most abundant renewable energy sources available, is gaining substantial traction [7]. While wind energy currently contributes only a fraction of the world's total power demand, its growth is accelerating rapidly [2]. Additionally, the cost per watt of electricity generated from wind is declining in tandem with its expansion [8]. This trend underscores the increasingly prominent role of wind energy integration (WEI) in our global transition toward cleaner and more sustainable

The associate editor coordinating the review of this manuscript and approving it for publication was Yonghao Gui[ID].

TABLE 1. Nomenclature table.

Variables	Description	Variables	Description
Wind power input	P_w	Gear Ratio	G
Wind turbine mechanical power	P_m	Wind Turbine Efficiency	η
Tip speed ratio	λ	Mass of the Air in Kg	m
Power coefficient	C_P	Wind Force in N-m	F
Air density in Kg/m^3	ρ	Gas Constant	R
Rotor swept area in m^2	S	Gravity Constant	g
Angular speed in radians	ω_t	Temperature in Kelvin	K
Rotor radius in meter	r	Aerodynamic Torque	Tr
Wind speed in m/sec	V	Moment of inertia	J
Tip speed ratio	λ_{opt}	Design constants	$c_1, c_2, c_3, c_4, c_5, c_6$
Power coefficient	D_T	Moment of inertia	J
Lumped uncertainty term	d_1	DC Link Voltage	E
Speed control input	T_{em}	Stator side DC link current	I_{os}
DC Voltage	E	Rotor side DC link current	I_{or}
Time derivative	h_1	Stator side Active Power	P_s
Speed Tracking error	e_1	Rotor side Active Power	P_r
Fractional operator	O^α	Stator side self inductance in Henry	L_s
Discontinuous gain of the controller	k_{r1}	Rotor side self-inductance in Henry	L_r
Design constants	c_7, and c_8	Rotor and Stator side mutual inductance in Henry	L_m
Actual DC link voltage	E^*	d-q reference frame stator side voltage	V_{ds}, V_{qs}
Time derivative of the error	$\dot{e}_E$	d-q reference frame stator side voltage	V_{dr}, V_{qr}
Air-gap power	P_δ	d-q reference frame stator side current	I_{ds}, I_{qs}
Discontinuous switching gain	k_{r2}, k_{r3}, k_{r4}	d-q reference frame rotor side current	I_{dr}, I_{qr}
The magnitudes of the wind unit	S_A	d-q reference frame stator Flux in Weber	$\varphi_{ds}, \varphi_{qs}$
PCC bus voltages	S_B	d-q reference frame rotor Flux, in Weber	$\varphi_{dr}, \varphi_{qr}$
Magnitude angle	Z	Stator side Reactive Power	Q_s
Phase angle	γ	Rotor side Reactive Power	Q_r
Frequency of the wind generator	f_o	Generator Speed	Ω_r
Amplitude of the wind generator	U_o	Current tracking error in d-axis	e_{Id}
Frequency droop coefficient	m	Current tracking error in q-axis	e_{Iq}
Indicative of the voltage droop coefficient	n	Rotor resistance in ohms	r_r
The nominal active power	P_n	Stator resistance in ohms	r_s
The nominal reactive power of the wind	Q_n	Number of pole pairs	p
Rotor power	(P_r)	d-q component current from GSC side	$I_d - I_q$
Stator power	(P_s)	Stator and Rotor angular speed	ω_s, ω_r
Number of turns	w	Reference generator speed	Ω_{r-ref}
Winding factor	ε	Generator Torque	T_t

power generation, and power system stability (PSS) [9], [10], [11].

Wind energy is harnessed by employing turbines that are linked to electrical generators. In the quest for optimizing power generation, variable-speed wind turbines employ adaptive shafts to track changes in wind speed effectively [8], [12], [13]. Additionally, the significance of generators cannot be overstated, as they play an equally vital role in facilitating the seamless integration of wind power into the grid. Wind energy conversion systems (WECSs) have emerged as an intriguing

solution for countries across the globe seeking to diversify their energy sources. This appeal stems from the inherent renewable and abundant nature of wind energy [3]. However, it's important to note that the conversion of wind energy is inherently stochastic due to the unpredictable variations in wind speed [14], [15].

Doubly Fed Induction Generators (DFIGs) find their niche in high-power wind generation systems (WGSs), especially in the context of variable-speed wind turbines [16]. In wind turbine applications where DFIGs are extensively utilized,

the rotor's rotational speed is dynamically adjusted to match varying wind speeds. DFIGs offer the versatility of operating in both hypo-synchronous and hyper-synchronous generator modes, making them a preferred choice for modern grid systems with fluctuating wind speeds. Compared to their fixed-speed counterparts like synchronous and induction generators, DFIGs present several advantages, including cost-efficient converters, minimal power losses, the capability for four-quadrant operation, and a wide range of speed operating capabilities [17], [18], [19], [20]. These attributes make them particularly well-suited for variable wind speed operations in contemporary grid systems.

Nonetheless, controlling grid-connected DFIGs presents a complex challenge due to the need to regulate active and reactive powers between the grid and DFIG-based wind generation systems (WGS) [21]. The essence of employing variable-speed technology in wind turbines lies in the ability to harness power efficiently across a wide range of wind speeds, thereby optimizing power generation for varying wind conditions [6], [22], [23]. In the realm of WECSs, DFIGs, especially when integrated with upward-oriented horizontal-axis wind turbines, play a dominant role in converting mechanical energy into electrical power. The control of DFIGs, achieved through the manipulation of wind turbine blade pitch angles, allows for precise regulation of the wind turbine generator's output power, even in the face of higher wind speeds [20], [24]. This capability ensures the efficient and reliable harnessing of wind energy for sustainable power generation.

Recent advancements in wind turbine and generator technologies have led to a significant reduction in the energy costs associated with wind farms (WFs) [24]. However, the widespread deployment of wind farms can pose challenges to power system stability (PSS). Additionally, the variability of wind generator output can lead to fluctuations in the frequency of power systems, impacting the operation of turbines. While wind farms are equipped with frequency relays to disconnect them in response to frequency disturbances, mass disconnections of generating units can result in power oscillations [25].

To address these challenges and enhance the stability of smart grid-integrated wind power systems, various artificial intelligence (AI) techniques have been extensively applied in power electronic converters and induction motor drives. These AI techniques, including fuzzy logic (FL), machine/deep learning, expert systems (ES), neural networks (NN), robotics, genetic algorithms (GA), and natural language processing, emulate human intellectual functions, enabling computers to achieve self-healing capabilities. Machine and deep learning methodologies, in particular, have the potential to provide affordable, accessible, and highly accurate diagnostic tools for addressing complex optimization issues such as variable wind speeds, non-linear load variations, power dispatch, and load control at the point of coupling [23], [26], [27], [28].

Artificial Neural Network (ANN) techniques are gaining prominence as an alternative to conventional approaches or as integral components of integrated systems. ANN techniques offer several advantages, including the ability to learn from examples, tolerance for noisy and incomplete data, the capacity to handle non-linear problems, and the capability to perform rapid forecasting and generalization once trained [23]. Artificial intelligence finds applications in diverse sectors, including engineering, economics, medicine, and the military. It has proven valuable for the modeling, identification, optimization, forecasting, and control of complex and nonlinear systems [6]. Table 1 includes an elaborate list of nomenclature utilised in the study.

The main contributions of this research encompass the creation of an Incremental Tuned GAN capable of predicting crucial wind energy parameters, resulting in more precise decision-making. This model achieves superior predictive accuracy by incorporating advanced techniques like adaptive discriminators and self-attention mechanisms. Additionally, the research focuses on optimizing grid stability through parameters like droop gain and fine-tuning control strategies for various types of generators in the context of renewable energy sources like wind farms. Importantly, the research establishes a continuous monitoring and adjustment process, ensuring efficient wind energy utilization by iteratively assessing wind farm conditions and adapting power injection into the grid when necessary [21].

The manuscript is structured into different segments. Section II provides an explanation of the procedures and the challenges associated with analyzing wind speed and direction. In Section III, an effective method for detecting wind speed direction is presented, which involves using incremental GAN, the results and findings of the method are illustrated in Section IV, and Section V describes the conclusion and future work of the research.

II. MOTIVATION
The motivation behind this research is to harness wind energy effectively and sustainably at various wind behavior as explained in sub-section B. By developing an advanced predictive model and optimizing grid stability, the study aims to enable the widespread use of clean wind power. This research aspires to contribute to a greener and more reliable energy future, reducing our dependence on fossil fuels and mitigating environmental impacts.

A. LITERATURE REVIEW
The authors aimed to enhance control in DFIG-based wind energy systems using AI-integrated Fractional Order Robust Control (FFORC) [3]. The FFORC technique reduces chattering, provides smooth power tracking, and exhibits minimal steady-state error, surpassing the Sliding Mode Control (SMC) system. Potential limitations of FFORC should be explored further for comprehensive assessment in practical applications.

The researchers in [8] aimed to highlight the effectiveness of artificial organic controllers (AOCs) in controlling variable-speed wind generators, specifically the doubly fed induction generator (DFIG) which results in higher power output, reduced pitch angle fluctuations, enhanced power efficiency, smoother startup, benefiting grid stability, blade durability, and sensitivity to wind variations but this model required further exploration of practical issues and scalability considerations.

In [5], the researchers aimed to improve control of Brushless Doubly-Fed Induction Generators (BDFIGs) in wind energy systems by introducing an adaptive fuzzy PID controller as compared to traditional control methods which enhanced the power generation quality and quantity under varying conditions, addressing limitations of fixed-parameter PID controllers.

In [23], the research authors aimed to investigate sub-synchronous oscillation (SSO) issues in grid-connected wind farms, particularly in wind turbines with doubly fed induction generators (DFIGs). This research offers insights into abnormal wind turbine operations and potential solutions through advanced control technologies, but this model leads to an increase in the cost and complexity of the generating unit.

The authors developed a DFIG-based wind energy system [24] and designed a generator speed controller to improve speed regulation in response to varying wind speeds. It combines system modeling and fuzzy logic-based PID control, showing that the fuzzy logic controller outperforms the traditional PID controller, enhancing generator speed regulation in the WECS but its implementation was limited due to its complexity.

In [27] the researchers developed a novel method for microgrid frequency control using DFIG and battery energy storage system (BESS), ensuring battery charge and stability after disturbances which preserves battery charge, and stabilizes microgrid frequency effectively but this model faced difficulty, that was identified in real-life conditions.

The authors in [29] investigated underestimated natural ventilation through small openings, particularly single and double-sided ones, aiming to distinguish between effective ventilation/purging flow rate (PFR) and bulk air flow rate (AFR). This model offers insights into natural ventilation, highlighting underestimations in low wind pressure scenarios and introducing ventilation effectiveness. However, this model could affect ventilation rates in real-world scenarios, potentially limiting its broader applicability.

In [30], the authors predicted wind speeds for individual turbines in a wind farm using a model that analyzes both time and spatial characteristics. The model effectively used spatiotemporal features, achieving accurate wind speed predictions for future periods, and outperforming existing models. However, this model faced high consumption over time.

The authors of reference [31] established that the distributed model predictive control (DMPC) enables the synchronized operation of the wind farm (WF) and the power grid with the objective of frequency management, albeit with the trade-off of increased complexity that entails the use of optimization techniques.

In their study, the authors of reference [32] analyzed the impact of frequency response control on the interaction between the wind energy conversion system (WECS) and the grid. They put forth a hybrid active damping technique for the wind farm (WF) to alleviate the presence of lightly damped modes that may arise. Nevertheless, this alternative approach may prove to be ineffective in situations where the operational point is variable.

The research scholars in [33] learned that when the grid frequency drops below the rated condition, virtual inertia control and WECS de-loading are needed to increase active power output. Hence, the researchers discussed advanced methodologies like predictive control and artificial intelligence can improve this combination by determining the back-to-back converter reference quantities.

The design aspects and building of a DFIG are described in detail using AC/DC/AC pulse width modulation (PWM) voltage source electronic regulators in the rotor side circuit and vector control used to both the GSC and the RSC without taking any abnormal condition into account [34], [35], [36], [37]. The comparison of proportional integral control and proportional distribution control for the regulation of reactive power in a wind farm is the exclusive focus of [38] and [39], which concludes that proportional integral is more resilient than proportional distribution control. While a supervisory system manages the active and reactive power of the entire wind generation system, a machine-learning control scheme confirms that set points at the level of the wind turbines are reached [40].

The limitations of the existing method can be overcome using the proposed Incremental Tuned Generative Adversarial Network (GAN) method. The proposed method overcomes the limitations caused by characterizing wind positions accurately in some unsupervised learning approaches by a wind attribute analysis. The capability to predict the wind characteristics is significant where some methods lag at this phase which is overcome using the 2-level fused discriminator and self-attention. The proposed model filters the parameters based on the following factors over time, performance enhancement and adaptability. The wind farm conditions are continuously monitored by the Incremental GAN monitors that permit optimal tuning to power injection into the grid and provide an efficient and reliable wind energy utilization.

B. CHALLENGES

Wind behavior is characterized by its inherent complexity, marked by continual fluctuations in wind speed, shifts in wind direction, and the presence of turbulence. Effectively predicting and responding to these dynamic changes in real-time presents a substantial challenge for AI algorithms [8].
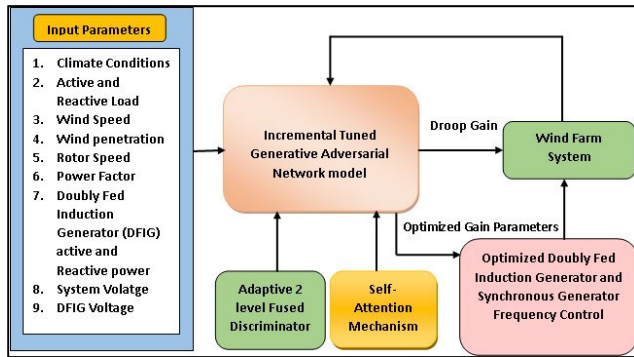
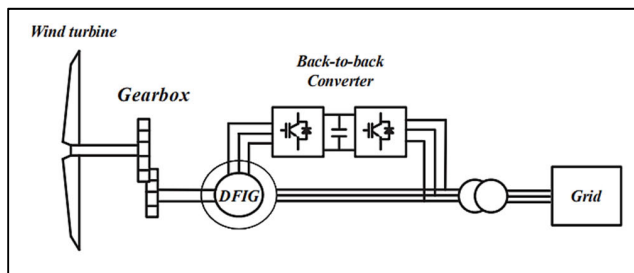**FIGURE 1.** Architecture of the proposed wind turbine farm model.

FIGURE 2. Operational concept of the wind energy system based on doubly fed induction generator.

FIGURE 3. Air velocity variation in an ideal model of a wind turbine.

-AI-driven systems are tasked with the intricate job of overseeing DFIG to maximize energy capture, all while upholding grid stability. The pursuit of achieving optimal control and synchronization between the wind turbine and the grid presents a complex and non-trivial challenge [6].

-DFIG-based wind turbines are prone to faults and failures, which have the potential to diminish their efficiency and overall lifespan. AI-based systems must possess the ability to detect and diagnose these faults proactively, facilitating timely maintenance interventions [20].

-Expanding AI-based solutions to encompass large wind farms equipped with multiple turbines presents its own set of challenges. Coordinating and optimizing the simultaneous operation of multiple turbines within a farm necessitates the application of advanced AI algorithms [25].

Wind turbines function in challenging environmental conditions, enduring extremes such as temperature fluctuations, high humidity levels, and exposure to saltwater in offshore installations. AI systems must demonstrate robustness, ensuring their resilience and reliability under these harsh circumstances [23].

-With the rising significance of AI in the realm of renewable energy, it becomes imperative to address ethical concerns about AI-driven decision-making and its potential consequences for local communities and wildlife [20].

III. METHODOLOGY

The primary objective of this research is to assess fluctuations in wind conditions and enhance the efficiency and reliability of wind energy generation and management through the provision of pre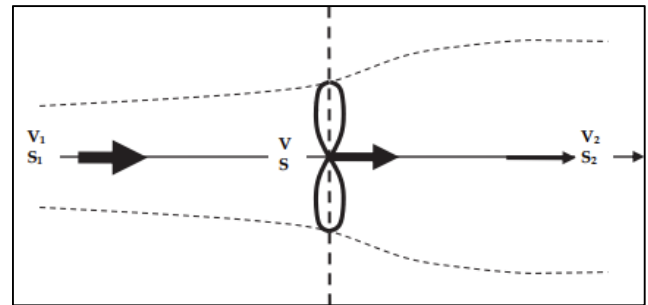cise and current wind data for informed decision-making. To achieve this, the authors proposed an incremental GAN model tailored for wind energy management as shown in Fig. 1, that utilizes parameters related to climate, load, wind speed, and wind penetration to predict gain parameters. The model undergoes incremental training and incorporates advanced components like an adaptive 2-level fused discriminator and a self-attention mechanism to amalgamate data from various sources, resulting in more accurate predictions of wind characteristics and power generation. For the purpose of estimating the wind resource potential for the existing wind farm, the researchers in [41] determined an average wind speed of 6.9 m/s at the wind turbine mast site. This allowed the meteodyne software to produce trustworthy simulation results. Accordingly, the present authors conducted their research using wind speeds ranging from 8 to 12 m/s. The design wind speed, V_{design}, should be 1.4 times the annual mean wind speed, V_{amws}, in accordance with the IEC61400-2 standard [42]. The Incremental Tuned GAN additionally generates important features, including droop gain and optimized gain parameters. The droop gain parameter regulates the speed at which a generator adjusts its output voltage and frequency in response to changes in load or generation, contributing to grid stability by redistributing the load among multiple WF generators. The research also focuses on parameter tuning for optimized control of DFIG and Synchronous Generators (SG), particularly important for grid stability when renewable energy sources like wind farms are present. The model continuously evaluates wind farm conditions, and if the criteria for power generation are not met, it iteratively reenters the Incremental Tuned GAN for further refinement, ensuring the efficient utilization of wind energy resources.

A. MODELING OF WIND ENERGY SYSTEMS

Fig. 2 illustrates the operational concept of the wind energy system based on DFIG. The system configuration is depicted in the block diagram, where the stator of the DFIG is directly linked to the grid, while its rotor is connected through back-to-back converters. Before devising a nonlinear controller for this wind energy system, it is crucial to first comprehend and derive the nonlinear mathematical models for both the Rotor Side Converter (RSC) and the Grid Side Converter (GSC) systems. The subsequent subsections will delve into

a comprehensive discussion of the mathematical models for wind turbines.

B. WIND TURBINE MODELING

At the Gottingen Institute in Germany, in the late 1920s, Albert Betz developed wind machine theory. A. Betz determined the maximum power a turbine rotor could generate from wind is 59.26% of the kinetic energy available in the wind. Consider the ideal wind rotor at rest in a fluid atmosphere, as seen in Fig. 3 [43]. The wind speed through the turbine rotor is defined as V (m/s), where the downwind cross-sectional area (S_2) is greater than the upwind cross-sectional area (S_1). The Betz equation addresses wind turbine efficiency restrictions by slowing the upstream wind speed (V_1) to its downstream speed (V_2) due to viscous and pressure drag on the rotor blades. The rotor extracts mechanical energy by lowering air stream kinetic energy from upwind to downwind or by breaking the wind flow. Assuming air flow is incompressible, the conservation of mass equation is [43]:

$$m = \rho S_1 V_1 = \rho S_2 V_2 = \text{constant} \qquad (1)$$

Euler's Theorem calculates wind force on the rotor as:

$$F = ma = m\frac{dV}{dt} = \rho SV(V_1 - V_2) \qquad (2)$$

Incremental work done by the air stream: $dE = Fdx$

Rotor power content of the wind stream P_r in watts [43]:

$$P_r = \frac{dE}{dt} = F\frac{dx}{dt} = FV \qquad (3)$$

Substituting the value of F from "(2)" in to "(3)", the power extracted by rotor P_r:

$$P_r = \rho SV^2 (V_1 - V_2) \qquad (4)$$

Ideal turbine power extraction P_m with $V_2 = {}^1/_3 V_1$ [43]:

$$P_m = P_{upwind} - P_{downwind} \qquad (5)$$

Wind power as a rate of change of kinetic energy:

$$P_w = \frac{\frac{1}{2}mV_1^2 - \frac{1}{2}mV_2^2}{\Delta t} = \frac{1}{2}\dot{m}\left(V_1^2 - V_2^2\right)$$
$$= \frac{1}{2}\rho SV(V_1 - V_2)(V_1 + V_2) \qquad (6)$$

Equating "(4)" and "(6)" implies that vind speed at the rotor cross section is the average of upper and lower wind speeds [44]:

$$\rho SV^2(V_1 - V_2) = \frac{1}{2}\rho SV(V_1 - V_2)(V_1 + V_2)$$
$$V = \frac{1}{2}(V_1 + V_2) \qquad (7)$$

By substituting tehvalue of V in "(4)" [44]:

$$P_r = \frac{1}{4}\rho SV(V_1 - V_2)^2(V_1 - V_2) \qquad (8)$$

$$P_r = \frac{1}{4}\rho SV(V_1)^2 - (V_2)^2(V_1 + V_2) \qquad (9)$$

And, therefore, coefficient of power can be computed by [44]:

$$C_p = \frac{\text{Power extracted by the rotor}}{\text{Total power of the wind stream}}$$
$$= \frac{\frac{1}{4}\rho SV(V_1)^2 - (V_2)^2(V_1 + V_2)}{\frac{1}{2}\rho SV^3} \qquad (10)$$

The interference ratio b is another way to express the ratio of V_2 to V_1.

$$b = \frac{V_2}{V_1} \qquad (11)$$

So, to express force as a function of interference ratio, we can say "2" as:

$$F = \frac{1}{2}\rho SV_1^2\left(1 - b^2\right) \qquad (12)$$

For any given interference factor b, we can express the extractable power P as:

$$P = \frac{1}{4}\rho SV_1^3\left(1 - b^2\right)(1 + b) \qquad (13)$$

The power coefficient can be written as follows in terms of b:

$$C_p = \frac{1}{2}\left(1 - b^2\right)(1 + b) \qquad (14)$$

By differentiating "(14)" with respect to 'b', we obtain:

$$\frac{d(C_p)}{db} = \frac{1}{2}\frac{d}{db}\left[\left(1 - b^2\right)(1 + b)\right] = \frac{1}{2}(1 - 3b)(1 + b) \qquad (15)$$

By, equating $\frac{d(C_p)}{db} = 0$, we can establish

$$\frac{1}{2}(1 - 3b)(1 + b) = 0$$
$$b = \frac{1}{3} = \frac{V_2}{V_1} \qquad (16)$$

This suggests that the downwind speed should be one-third of the upwind speed for the wind turbine to operate at its best.

Hence, the maximum coefficient of performance [44]:

$$C_{p\_max} = \frac{1}{2}\left[1 - \left(\frac{1}{3}\right)^2\right]\left(1 + \frac{1}{3}\right)$$
$$C_{p\_max} = 59.26\% \qquad (17)$$

C_{p_opt} is known as the Betz limit, which specifies the greatest amount of wind energy that may be transformed into rotational energy by the ideal wind turbine.

The authors considered the reference value of air density at 15 degrees celsius and sea level as 1.225 kg/m3. This is the International Standard Atmosphere's (ISA) value. the rotor swept area is 18.134 m^2 and the power coefficient is 0.48 [45]. The square of the rotor diameter and the cube of the wind speed increase the value of P_r considerably. Above sea level, air density depends on pressure and temperature [46].

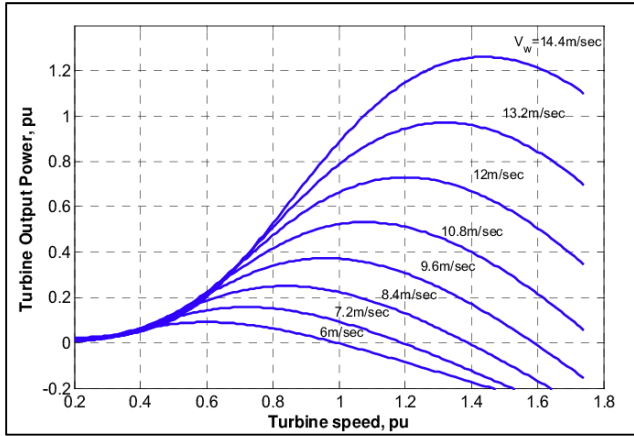$$\rho_z = \frac{\rho_o}{RT}exp\left(\frac{-gz}{RT}\right) \qquad (18)$$

FIGURE 4. Schematic representation of the wind turbine characteristics.

where ρ_Z is the air density as a function of altitude in kg/m3, ρ is the standard sea-level atmospheric density in Kg/m3, R is the air-specific gas constant 287.05 J/Kg-K, g is the gravity constant 9.81 m/s^2, T is the temperature Kelvin, and z is the altitude above sea level in meters [43]:

The formula for the tip speed ratio λ is expressed as follows:

$$\lambda = \frac{\omega_t r}{V} \qquad (19)$$

The tip speed ratio λ_{opt} plays a pivotal role in determining the maximum power output of a wind turbine at a given wind speed. Specifically, when $\lambda = \lambda_{max}$, the power coefficient C_p attains its maximum value, denoted as $C_P = C_{P-max}$. In this study, the power performance of the WECS is characterized by the relationship between C_P and λ. The aerodynamic torque T_r generated within the wind turbine with a gear ratio G, and the angular speed ω_t, is expressed as follows, underlining its significance in the system's overall performance [3]:

$$P = \frac{1}{2}\rho C_{p\_max} S V_1^3 \qquad (20)$$

$$T_r = \frac{T_t \omega_t}{G} = \frac{\omega_r}{G} \qquad (21)$$

By equating "(19)", "(20)" and "(21)", which represent the reference rotor speed ω_r and power as follows [3]:

$$\omega_{r-ref} = \frac{\lambda_{opt} G_v}{R} \qquad (22)$$

$$P_{grid-ref} = \frac{1}{2}\eta\rho r^2 C_{P-max} v^3 \qquad (23)$$

where the wind turbine efficiency is denoted as η.

C. DFIG SYSTEM MODELING

In this section, the mathematical model delves into the meticulous derivation of the robust control system, which encompasses both RSC and GSC converters.

Fig. 5 shows the DFIG equivalent circuit in the d-q reference frame. Assuming the DFIG's electrical modelling within the d-q reference frame is feasible. The voltage, flux, and power of the grid side and rotor side converters for
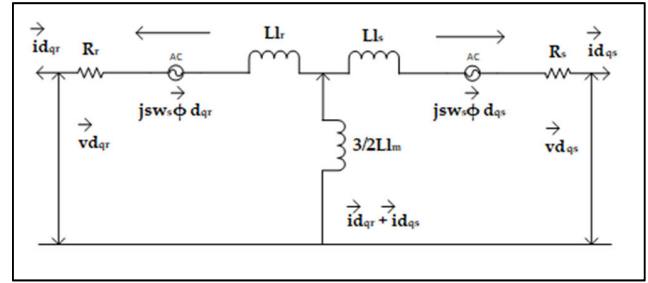

FIGURE 5. The representation of a DFIG in a synchronous d - q reference frame [47].

DFIG-based wind energy systems can be described in the d-q reference frame using the following equations [48].

$$V_{ds} = R_s I_{ds} + \dot{\varphi_{ds}} - \omega_s \varphi_{qs} \qquad (24)$$

$$V_{qs} = R_s I_{qs} + \dot{\varphi_{qs}} + \omega_s \varphi_{ds} \qquad (25)$$

$$V_{dr} = R_r I_{dr} + \dot{\varphi_{dr}} - \omega_r \varphi_{qr} \qquad (26)$$

$$V_{qr} = R_r I_{qr} + \dot{\varphi_{qr}} + \omega_r \varphi_{dr} \qquad (27)$$

$$\varphi_{ds} = L_s I_{ds} + L_m I_{dr} \qquad (28)$$

$$\varphi_{qs} = L_s I_{qs} + L_m I_{qr} \qquad (29)$$

$$\varphi_{dr} = L_r I_{dr} + L_m I_{ds} \qquad (30)$$

$$\varphi_{qr} = L_r I_{qr} + L_m I_{qs} \qquad (31)$$

The self-inductance coefficient of the stator and rotor windings is shown by L_s and L_r, where R_s and R_r are the stator and rotor resistances. The mutual coupling coefficient between the rotor and stator is represented by the symbol L_m. In the d-q park reference frame, the voltage and current components of the stator and rotor side are designated as V_{ds}, V_{qs}, I_{ds}, I_{qs}, V_{dr}, V_{qr}, I_{dr} and I_{qr} provides the electromagnetic torque equation per unit as stated in the d-q park reference [48]. The researchers in [49] displayed the machine modelling at varying wind speed in phase domain model and d-q reference frames. Additionally, six-phase transformer, grid-side converter, and rotor-side converter modelling has shown an improved reliability, performance, and less pulsing torque as the key benefits for asymmetrical six phase doubly fed induction generator (ASPDFIG). The researchers in [50] provided a hybrid strategy for DFIG-based wind power systems that improves control efficiency with quantum process and deep reinforcement learning (QPDRL). The proposed QPDRL avoided the local optimal solutions, detected critical phases, and updated the DFIG regulating algorithms online. The system showed an improved performance, by reducing the DC link voltage ripples by 62% and speed overshoot by 99%. Based on the research [48], and [49] outcomes, the authors considered the six phase DFIG control system should be the future work space.

D. CONTROL SYSTEM FOR RSC CONVERTERS

Two control schemes, the speed controller, and the d - q axis current controllers, are derived in this subsection.

1) SPEED CONTROLLER

The phrase rotor angular speed ω_r, in terms of generator speed Ω_r is written like:

$$\omega_r = P\Omega_r \tag{32}$$

The rotor aerodynamic torque-speed (T_r - Ω_r) relationship, sometimes known as the DFIG mechanical equation, is as follows [3]:

$$J\frac{d}{dt}\Omega_r = T_{em} - T_r - f_r\Omega_r \tag{33}$$

where the phrase electromagnetic torque T_{em} in terms of rotor d-q axis fluxes φ_{ds}, and φ_{qs} is written as [3]:

$$T_{em} = P\frac{L_m}{L_s}\left(\varphi_{qs}I_{dr} - \varphi_{ds}I_{qr}\right) - T_r - f_r\Omega_r \tag{34}$$

Taking into consideration the relationship below to simplify the above expression:

$$\varphi_{ds} = \varphi_s, \quad \varphi_{qs} = 0 \tag{35}$$

The expression that results from combining "(34)" and "(35)" is as follows:

$$T_{em} = P\frac{L_m V_s}{\omega_s L_s}I_{qr} \tag{36}$$

The expression for the d/q stator voltage vectors under constant stator flux and per-phase resistance is as follows [3]:

$$V_{ds} = 0, \quad V_{qs} = V_s = \omega_s\varphi_s \tag{37}$$

The d/q voltages in the rotor axis V_{dr}, V_{qr} and stator side active-reactive powers P_s, Q_s are expressed in terms of rotor current I_r as follows by combining "(24)", "(25)", "(26)", "(27)" and "(28)", "(29)", "(30)", "(31)":

$$V_{dr} = R_r^*I_{dr} + \sigma L_r\frac{d}{dt}I_{dr} - \sigma L_r s\omega_s I_{qr} \tag{38}$$

$$V_{qr} = R_r^*I_{qr} + \sigma L_r\frac{d}{dt}I_{qr} - \sigma s\omega_s I_{dr} + s\frac{L_m V_s}{L_s} \tag{39}$$

$$P_s = -\frac{L_m V_s}{L_s}I_{qr} \tag{40}$$

$$Q_s = \frac{V_s^2}{\omega_s L_s} - \frac{L_m V_s}{L_s}I_{dr} \tag{41}$$

where σ and s are defined as follows:

$$\sigma = 1 - \frac{L_m}{L_r L_s}, \quad and \quad s = \frac{\omega_s - \omega_r}{\omega_s} \tag{42}$$

Here, s stands for the DFIG slip. The nonlinear system model is described as follows using the equations mentioned above:

$$\dot{X} = A(x) + B(u) = a(x) + \Delta a + bu + \Delta bu \tag{43}$$

$$\dot{X} = A(x) + B(u) = a(x) + bu + d(t) \tag{44}$$

In this case, $u = [u_1, u_2] = [V_{dr}, V_{qr}]^T$, and $X = [I_{dr}, I_{qr}]^T$, a and b represent the best approximation (nominal model) of A and B respectively; Δa, and Δb denote plant and input vector uncertainties, whereas $d = \Delta a + \Delta bu = [d_{I_d}, d_{I_q}]^T$ is the system models unknown lumped uncertainty.

The derivation process begins with the development of the speed controller, which is rooted in the dynamic model. The pulse width modulation controller is used for controlling RSC and GSC. This dynamic model in "(33)" is then reformulated and expressed as follows [3]:

$$\frac{d}{dt}\Omega_r = \frac{T_{em}}{J} + d_1 \tag{45}$$

In this context, a key element known as the lumped uncertainty term is being introduced, which denotes as d_1. This uncertainty term is precisely represented by the equation [3]:

$$d_1 = -\frac{T_r}{J} - \frac{f_r\Omega_r}{J} \tag{46}$$

Now, within the context of "(45)", it's important to note that T_{em} stands for the control input while J represents the moment of inertia. Furthermore, formally define the speed tracking error e_1 in the following manner [3]:

$$e_1 = \Omega_r - \Omega_{r-ref} \tag{47}$$

The time derivative of h_1 can be expressed $\dot{e}_1 = \dot{\Omega}_r - \dot{\Omega}_{r-ref}$ By substituting "(45)" in $\dot{e}_1$ to obtain a modified expression as follows [3]:

$$\dot{e}_1 = \frac{T_{em}}{J} + d_1 - \dot{\Omega}_{r-ref} \tag{48}$$

To formulate the speed controller, we opt for a fractional-order sliding surface, expressed as follows [3]:

$$S_1 = c_1 O^{-\alpha}e_1 + c_2\int \dot{e}_1 \tag{49}$$

In this context, the variables c_1, and c_2 stand as design constants for the sliding surface. By applying the fractional operator O^α to "(49)", derive the following expression [3]:

$$O^\alpha S_1 = c_1 e_1 + c_2 O^{\alpha-1}\dot{e}_1 \tag{50}$$

Upon combining "(48)" with "(50)", obtain the modified relation as follows:

$$O^\alpha S_1 = ce_1 + c_2 O^{\alpha-1}\left[\frac{T_{em}}{J} + d_1 - \dot{\Omega}_{r-ref}\right] \tag{51}$$

From "(51)", we derive the speed controller as follows [3]:

$$\begin{cases} T_{em} = T_{em-eq} + T_{em-s} \\ T_{em-eq} = J\left(\dot{\Omega}_{r-ref} - O^{1-\alpha}\frac{c_1}{c_2}e_1\right) \\ T_{em-s} = J\left(-\frac{k_{r1}}{c_2}O^{1-\alpha}sgn(S_1)\right) \end{cases} \tag{52}$$

"Equation (52) introduces k_{r1} as the discontinuous gain parameter of the controller. Notably, within the term, T_{em-s} there is a fractional derivative that considers the magnitude $(O^{1-\alpha})$. This specific inclusion plays a pivotal role in dampening the chattering phenomena, ultimately contributing to improved overall control performance.

2) D-Q AXIS CURRENT CONTROL

First, the expressions of active power P and reactive power Q are expressed as follows in order to derive the d and q axis current controllers:

$$I_{qr-ref} = \frac{\omega_s L_s}{P L_m V_s} T_{em-ref} \tag{53}$$

$$Q_{ref} = \frac{V_s^2}{\omega_s L_s} - \frac{L_m V_s}{L_s} I_{dr-ref} \tag{54}$$

With $Q_{ref} = 0$, reference d-axis current is expressed as

$$I_{dr-ref} = \frac{V_s}{L_m \omega_s} T_{em-ref} \tag{55}$$

The following defines the current tracking faults on the d and q axes:

$$e_2 = \begin{bmatrix} e_{I_d} & e_{I_q} \end{bmatrix}^T = \begin{bmatrix} I_{dr} - I_{dr-ref} & I_{qr} - I_{qr-ref} \end{bmatrix}^T \tag{56}$$

$$\dot{e}_2 = \dot{x} - \dot{x}_{ref} = a(x) + bu + d - \dot{x}_{ref} \tag{57}$$

The fractional order sliding surface S, with c_3; c_4; c_5 and c_6 are the design parameters:

$$S = \begin{bmatrix} S_2 \\ S_3 \end{bmatrix} = \begin{bmatrix} c_3 O^{-\alpha} e_{I_d} + c_4 \int \dot{e}_{I_d} \\ c_5 O^{-\alpha} e_{I_q} + c_6 \int \dot{e}_{I_q} \end{bmatrix} \tag{58}$$

By applying the fractional operator O^a to "(58)", the resultant expression:

$$O^\alpha S = \begin{bmatrix} O^\alpha S_2 \\ O^\alpha S_3 \end{bmatrix} = \begin{bmatrix} c_3 e_{I_d} + c_4 O^{\alpha-1} \dot{e}_{I_d} \\ c_5 e_{I_q} + c_6 O^{\alpha-1} \dot{e}_{I_q} \end{bmatrix} \tag{59}$$

Hence, the equivalent control terms

$$u_{eq} = \begin{bmatrix} u_{eq1} \\ u_{eq2} \end{bmatrix} = \begin{bmatrix} b^{-1} \left(-a(x) + \dot{I}_{d-ref} - \frac{c_3 O^{1-\alpha} e_{I_d}}{c_4} \right) \\ b^{-1} \left(-a(x) + \dot{I}_{qr-ref} - \frac{c_5 O^{1-\alpha} e_{I_q}}{c_6} \right) \end{bmatrix} \tag{60}$$

$$u_s = \begin{bmatrix} u_{s1} \\ u_{s2} \end{bmatrix} = \begin{bmatrix} b^{-1} \left[\frac{-k_{r2} O^{1-\alpha} sgn(S_2)}{c_4} \right] \\ b^{-1} \left[\frac{-k_{r3} O^{1-\alpha} sgn(S_3)}{c_6} \right] \end{bmatrix} \tag{61}$$

The sliding condition is achieved by assigning values to Setting $k_r = \begin{bmatrix} k_{r2} & k_{r3} \end{bmatrix} > d_{max}$ where d_{max} denotes the maximum limit of the disturbance and it is assumed that this limit is known.

Certainly, Fig. 4 provides a schematic representation of the wind turbine characteristics under specific conditions. At a wind speed of 5 meters per second (5m/s), the wind turbine exhibits its operating parameters. The maximum revolutions per minute (RPM) for this wind turbine model is limited to 1500, and it achieves a maximum power output of 0.5 per unit under these conditions. This figure serves as an essential visual reference to understand the wind turbine's behavior and performance at the specified wind speed and its corresponding power generation capabilities.

E. FORMULATION OF DC LINK MODELING AND GRID-SIDE CONTROL

Throughout the control operation, the DC link voltage is maintained by the DC link capacitor that is linked between the RSC and GSC converters. Without changing the DC link voltage, the GSC converter side controls the active power (P) and reactive power (Q). This can be accomplished by applying a traditional vector control method by lining up the reference frame with the grid or stator voltage vector. Consequently, $V_d = V_s$, and $V_q = 0$.

As a result, the following formulas are used for P and Q.

$$P_s = \left(\frac{3}{2} \right) (V_{ds} I_{ds} + V_{qs} I_{qs}) = \frac{3}{2} (V_{ds} I_{ds}) \tag{62}$$

$$Q_s = \left(\frac{3}{2} \right) (V_{ds} I_{ds} - V_{ds} I_{qs}) = -\frac{3}{2} (V_{ds} I_{ds}) \tag{63}$$

The ratio of current component I_d to active power and current component I_q to reactive power flowing between the GSC converter and the grid is represented by "(62)", and "(63)".

$$EI_{os} = \frac{3}{2} V_d I_d \tag{64}$$

where, E represents the DC link voltage, I_{os} is the stator side, and I_{or} is the rotor side DC link current. Additionally, the following shift in rotor side DC power equals the GSC converter-grid active power.

$$C \frac{dE}{dt} = I_{os} - I_{or} \tag{65}$$

Upon combining "(64)" with "(65)", obtain the modified relation as follows:

$$\dot{E} = \frac{1}{C} \left(\frac{3}{2E} V_d I_d - I_{or} \right) \tag{66}$$

$$\dot{E} = g(x) I_d - \frac{1}{C} I_{or} \tag{67}$$

$$\dot{E} = (\Delta g(x) + g_o(x)) I_d - \frac{1}{C} I_{or} \tag{68}$$

$$\dot{E} = g_o(x) I_d - \frac{1}{C} I_{or} + d_E \tag{69}$$

Here, $d_E = \Delta g(x) I_d$, represents an uncertainty term.

To maintain a constant DC link voltage, the mathematical model calculates the error by taking the difference between the reference DC voltage and the actual DC link voltage, which is expressed as follows [3]:

$$e_E = E - E^* \tag{70}$$

The time derivative of the error in the equation above is expressed as follows:

$$\dot{e}_E = \dot{E} - \dot{E}^* \tag{71}$$

Upon substituting the expression for $\dot{E}$ into "(71)", the resulting expanded expression is as follows [3]:

$$\dot{e}_E = g_o(x) I_d - \frac{1}{C} I_{or} + d_E - \dot{E}^* \tag{72}$$

To regulate the DC link voltage effectively, here opt for a fractional calculus-based sliding surface described by "(73)":

$$S_E = c_7 O^{-\alpha} e_E + c_8 \int \dot{e}_E \tag{73}$$

Upon applying the operator O^α to both sides of "(73)", the resulting relation is as follows [3]:

$$O^\alpha S_E = c_7 e_E + c_8 O^{\alpha-1} \dot{e}_E \tag{74}$$

By combining "(73)" with "(74)", obtain the following expanded relation:

$$O^\alpha S_E = c_7 e_E + c_8 O^{\alpha-1} \dot{e}_E \left(g_o(x) I_d - \frac{1}{C} I_{or} + d_E - \dot{E}^* \right) \tag{75}$$

Utilizing "(75)", the control law can be defined as follows [3]:

$$\begin{cases} I_d = I_{deq} + I_{ds} \\ I_{deq} = \frac{1}{go(x)} \left\{ \dot{E}^* + \frac{1}{c_7} I_{or} - \frac{c_7}{c_8} O^{1-\alpha}(e_E) \right\} \\ I_{ds} = \frac{1}{go(x)} \left(-\frac{k_{r4}}{c_8} O^{1-\alpha}(sgn(S_E)) \right) \end{cases} \tag{76}$$

"In "(76)" c_7, and c_8 serves as the design parameters while, k_{r4} representing the discontinuous switching gain. This formulation captures the key components of the "(76)", allowing for precise control system design and parameter tuning.

F. PRELIMINARIES
Climatic conditions in wind farms, along with other input parameters like load (active and reactive power), wind speed, wind penetration, rotor speed, power factor (PF) and DFIG active and reactive collectively influence the performance and operation of wind energy systems. Here's how each of these parameters can impact wind farms:

1) CLIMATIC CONDITIONS
Climatic conditions, including temperature, humidity, air density, and extreme weather events, directly affect wind turbine performance and efficiency. For example, higher temperatures reduce air density, which can affect energy generation. Severe weather events such as storms or ice accumulation can lead to downtime and maintenance needs.

2) LOAD (ACTIVE AND REACTIVE POWER)
Load refers to the amount of electrical power consumed by connected devices or systems. In a wind farm, variations in active power demand can impact the stability of the electrical grid. Reactive power is also important for maintaining voltage levels and ensuring the grid's reliability. Wind turbines may need to provide both active and reactive power support to meet load requirements and grid regulations.

3) WIND SPEED
Wind speed is a crucial factor in wind energy generation. Higher wind speeds generally lead to greater energy output, while low or variable wind speeds can reduce power production. Wind speed data is essential for optimizing turbine operation and ensuring grid integration.

4) WIND PENETRATION
Wind penetration refers to the percentage of total electricity generation supplied by wind energy within a given area or grid. High wind penetration can introduce challenges related to grid stability, voltage regulation, and the need for energy storage or backup power sources during periods of low wind generation.

5) ROTOR SPEED
The rotor speed of wind turbines must be controlled to maximize energy capture and prevent damage due to overspeed. Adjusting rotor speed based on wind conditions is essential for optimizing power generation and ensuring turbine longevity.

6) POWER FACTOR (PF)
The power factor represents the ratio of real power (active power) to apparent power in an electrical system. Wind turbines and wind farms often need to maintain a specific power factor to ensure grid compatibility and meet grid codes. Control systems may adjust the power factor to maintain grid stability.

7) DFIG ACTIVE AND REACTIVE POWER
The active and reactive power output of the DFIG is essential for grid compatibility. Control of these parameters ensures that wind farms can meet grid requirements and contribute to grid stability.

Overall, these input parameters, when properly monitored and controlled, allow wind farms to operate efficiently, contribute to grid stability, and integrate renewable energy into the electrical grid effectively. Managing these parameters is critical for the successful deployment and operation of wind energy systems.

G. DROOP CONTROL MATHEMATICAL MODEL
The droop gain parameter regulates the speed at which a generator adjusts its output voltage and frequency in response to changes in load or generation, contributing to grid stability by redistributing the load among multiple wind farm generators. Each DFIG-WT can be depicted as a voltage source connected to a shared bus via line impedance denoted as Z. The power transfer from the wind unit to the Point of Common Coupling (PCC) bus can be expressed as follows [51]:

$$S_A = P_A + jQ_A = U_{A e^{j\delta_p}} \left(\frac{U_A e^{-j\delta_p} - U_B}{Z e^{-j\gamma}} \right) \tag{77}$$

$$S_A = \frac{U_A^2}{Z} e^{j\gamma} - \frac{U_A U_B}{Z} e^{j(\gamma + \delta_p)} \tag{78}$$

In this context, S_A and S_B correspond to the magnitudes of the wind unit and PCC bus voltages, while Z and γ respectively signify the magnitude and phase angle of the line impedance. Furthermore, $Ze^{j\gamma} = R + jX$, and δ_p which characterizes the power angle. To establish the voltage difference, the model employs $\Delta U = U_A - U_B$ [51].

$$\Delta U = \frac{1}{U_A}(RP_A + XQ_A) \quad (79)$$

$$\delta_p = \frac{1}{U_A U_B}(XP_A - RQ_A) \quad (80)$$

"Equations (79) and "(80)" illustrate the decoupling of $(P - Q)$ from each other solely through $\delta_p - \Delta U$, but this scenario holds only in an ideal case specifically, in cases where there is either pure inductance $(X = 0)$ or pure resistance $(R = 0)$. When apply $(R = 0)$ to "(79)" and "(80)", the following outcome emerges [51]:

$$P_A = U_A U_B \delta_p / X \quad (81)$$

$$Q_A = U_A \Delta U / X \quad (82)$$

Under these conditions, the conventional droop-sharing scheme can be deployed to control and regulate the active and reactive power output of the wind turbine generator unit as follows [51]:

$$f = f_o - mP \quad (83)$$

$$U = U_o - nQ \quad (84)$$

Here f_o and U_o parameters are associated with the frequency and amplitude of the wind turbine generator unit voltage at no load (set points). The droop coefficients for these parameters can be described as follows: m is assigned to the frequency droop coefficient and n is indicative of the voltage droop coefficient [51].

$$m = \Delta f / P_n \quad (85)$$

$$n = \Delta U / Q_n \quad (86)$$

In this context, P_n represents the nominal active power, and Q_n represents the nominal reactive power of the wind unit. Usually, there exist permissible deviations of up to 2% for Δf and 5% for ΔU. It is a standard practice to maintain Δf, and ΔU as equal values across all units.

$$\Delta f = mP_{n1} = m_2 P_{n2} = \ldots\ldots\ldots = m_j P_{nj} \quad (87)$$

$$\Delta U = n_1 Q_{n1} = n_2 Q_{n2} = \ldots\ldots\ldots = n_j Q_{nj} \quad (88)$$

Consequently, the coefficients exhibit an inverse relationship with nominal powers, choosing the droop coefficients following "(87)" and "(88)" guarantees that each unit contributes to power sharing in alignment with its designated nominal rating [51].

H. ADAPTIVE SELF ATTENTION-BASED GAN NETWORK

As shown in Fig. 6, the authors provide a more detailed explanation of how the GAN is employed in the research to enhance wind energy generation and management, with a
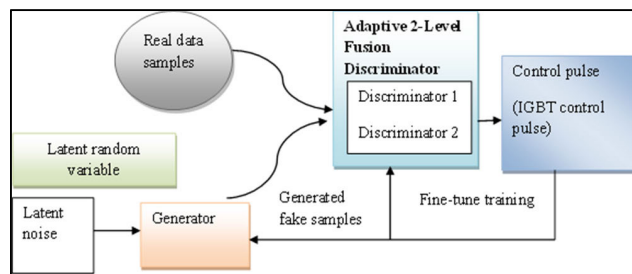

FIGURE 6. The architecture of the incremental GAN model.

focus on the discriminator's novelty, adaptive 2-level fusion, and the integration of the self-attention mechanism. In this research, the incremental GAN comprises two main components: the generator and the discriminator. The generator aims to create accurate and up-to-date wind data, including parameters like wind speed, direction, robustness, and power generation. The discriminator plays a critical role in assessing the quality and authenticity of the generated data, in this research, enhancing the discriminator makes it more effective at distinguishing between real and generated data.

1) WORKING OF THE ADAPTIVE 2-LEVEL FUSION DISCRIMINATOR

-Level 1 (Primary Discriminator - Discriminator-1): Discriminator-1 assesses the predictions made by the generator (GAN's Generator). It takes the generated data as input and compares it to real data, evaluating how closely the generated data matches the actual observations. It calculates a loss based on the discrepancy between real and generated data. This loss is used as feedback to update and improve the generator's parameters.

-Level 2 (Secondary Discriminator - Discriminator-2): Discriminator-2 operates at a higher level and evaluates the assessments made by Discriminator-1. It examines not only the differences between real and generated data but also considers other features, such as the distribution of data points. It calculates a secondary loss based on the discrepancies identified by Discriminator-1 and other relevant information. The outputs (losses) of Discriminator-1 and Discriminator-2 are fused or combined to create a unified assessment of the incremental GAN model's performance. Both Discriminator-1 and Discriminator-2 are trained to become more proficient at assessing the quality of generated data. The incremental GAN model's generator uses a combination of D1 loss and D2 loss as feedback to update its parameters and improve its data generation.

2) SELF ATTENTION MECHANISM

The self-attention mechanism is a neural network component that plays a critical role in enhancing the discriminator's and generator's capabilities by selectively focusing on important features in the input data.

It helps improve the model's understanding of relationships between different data points, leading to more accurate predictions. Self-attention mechanisms analyze the relationships

between different elements in the data (e.g., features like wind speed, load, and temperature). The self-attention mechanisms assign different attention weights to these elements, allowing the model to focus more on relevant information while downplaying less important details. By attending to the most informative features, the self-attention mechanism helps the discriminator make better assessments and the generator creates more realistic data. Finally, this study focused on the originality of the discriminator, using the self-attention mechanism, and implementing an adaptive 2-level fusion mechanism to improve the performance of the incremental GAN model in wind turbine applications. These components work together to improve the incremental GAN model's ability to generate accurate and realistic data, which is crucial for optimizing wind turbine operations, including parameters like droop gain. The generator and the discriminator are classified as:

Generator = [Sequence Input Layer (7), Fully Connected Layer (64), Relu Layer (1), Fully Connected Layer (1), Tanh Layer (1)].

Discriminator = [Sequence Input Layer (1), Fully Connected Layer (64), Relu Layer (1), Fully Connected Layer (1), Regression Layer (1)].

Using a fully connected neural layers with high-dimensional input data might result in a substantial rise in the parameter count, rendering it computationally expensive and perhaps impracticable for training. Therefore, the authors have chosen to utilise 64 neurons in the fully connected layers to meet the special criteria of the neural network architecture in this situation, as it is compatible with high-dimensional data.

IV. CONTROL STRATEGIES FOR GRID-TIED DOUBLY FED INDUCTION GENERATOR (DFIG) AND SYNCHRONOUS GENERATOR (SG)

Incremental tuning of a GAN optimizes the grid-integrated DFIG and SG systems by training the generator to create accurate data resembling real parameters, while the discriminator assesses and minimizes discrepancies between the generated and real data. Iterative training refines the generator's output, improving authenticity. This enhanced data benefits control algorithms, predictive maintenance, and optimization of DFIG and SG systems, enhancing wind energy power generation efficiency and reliability. DFIG and SG are two types of generators commonly used in wind farms.

A precise control strategy is essential to ensure these generators operate effectively and contribute to grid stability. For DFIG, control strategies may involve adjusting rotor speeds and power factors to match grid requirements. SGs, on the other hand, may use governor control and excitation control to regulate output power and maintain grid frequency.

A. DFIG CONTROL SYSTEM

The DFIG is distinguished by its sturdy and widely recognized design. In this configuration, the stator is directly connected to the grid, while the rotor is linked to the mains via an inverter. One notable advantage is the use of a

relatively small inverter, which only channels the air-gap power, denoted as P_δ, into the grid. Additionally, the grid choke can be sized to accommodate the lower rotor current. However, this doubly-fed induction generator concept does introduce certain unique features, such as direct harmonic emissions from the stator, when compared to other types of generators. Nonetheless, the DFIG is a well-established principle, and its fundamental equations have been extensively documented and published in [52], [53].

$$u_{si} = r_s.i_{si} + \frac{d\Psi si}{dt}, \ where \ i = 1, 2, 3\ldots. \quad (89)$$

$$u_{ri} = r_r.i_{ri} + \frac{d\Psi ri}{dt} \quad (90)$$

$$T_{el} = \frac{P}{2}\sum_{i=1}^{3} i_i.\frac{d\Psi_i}{dv} \quad (91)$$

$$n = \frac{60.(f_s + f_r)}{P} \quad (92)$$

(P, is the total count of pole pairs)

$$u_d = r_s.i_d + \frac{d\Psi_d}{dt} - \Omega_e\Psi_q \quad (93)$$

$$u_q = r_s.i_q + \frac{d\Psi_q}{dt} - \Omega_e\Psi_d \quad (94)$$

$$\Omega_e = P.\Omega_{mech} \quad (95)$$

In the $(d-q)$ reference frame, the calculation of active power (P) and reactive power (Q) is as follows [52]:

$$P = 3.\left(u_d.i_d + u_q.i_q\right) \quad (96)$$

$$Q = 3.\left(u_d.i_q + u_q.i_d\right) \quad (97)$$

The relationship between stator power (P_s) and rotor power (P_r) is expressed in terms of parameters such as the number of turns w and winding factor ε [52]:

$$\frac{P_s}{P_r} = \frac{w_s\varepsilon_s f_s}{w_r\varepsilon_r f_r} \quad (98)$$

Under identical rotor and stator current conditions, the DFIG can provide twice the power output when compared to an asynchronous generator equipped with a squirrel-cage rotor [52].

$$P = 2.U_1.I_1.\cos\phi_1 \quad (99)$$

Harmonics are generated both by the grid-side inverter and the rotor-side inverter. These switching distortions are subsequently transferred to the stator side and directly injected into the grid. The fundamental frequency on the grid side remains constant at 50 Hz, while the harmonics depend on both the pulse number (for current harmonics) and the pulse frequency (for voltage harmonics). The rotor harmonics operate under the same principles, but they transform the grid side. This transformation introduces a phase shift, which is contingent on the instantaneous speed and the machine's inductance. The outcome is the emergence of transformed rotor harmonic frequencies, denoted as $f_{tr-rotor}$ which manifests as interharmonics on the grid side. These inter-harmonics can be derived

from the rotor frequency f_{rotor} and the mechanical frequency f_{mech} [52].

$$f_{tr-rotor_n} = f_{rotor_n} + f_{mech} \qquad (100)$$

(n, which is a multiple of the rotor-side fundamental).

On the grid side, anticipate the presence of harmonics with sidebands originating from the grid-side inverter, as well as interharmonics resulting from the transformation process occurring within the generator itself, courtesy of the rotor-side inverter. Sidebands of voltage harmonics are generated due to amplitude modulation effects. Furthermore, inter-harmonics arise because of load-dependent variations in the switching of both the grid-side and rotor-side inverters.

Consequently, during dynamic WEC operations, it's not always feasible to establish a direct correlation between rotor switching and grid-side inter-harmonics. Table 2 summarizes the DFIG specifications used in the simulation exercise.

B. SG CONTROL SYSTEM

In contrast to the induction machine, the SG operates in a fully decoupled manner from the grid using an inverter. The fundamental equations governing the behavior of the SG are as follows [52]:

$$u_{si} = r_s.i_{si} + \frac{d\Psi si}{dt} \qquad (101)$$

The stator system, as per "(37)" converting into a self-contained, revolving frame of reference leads to:

$$u_k = r_s.i_k + \frac{d\Psi_k}{dt} + j.\Omega_e\Psi_k \qquad (102)$$

With

$$\Omega_e = p\Omega_{mech} \qquad (103)$$

In the $(d-q)$ reference frame, derive the U_d, and U_q voltages to calculate the T_t torque [52].

$$u_d = r_s.i_d + \frac{d\Psi_d}{dt} - \Omega_e\Psi_q \qquad (104)$$

$$u_q = r_s.i_q + \frac{c\Psi_q}{dt} - \Omega_e\Psi_d \qquad (105)$$

$$T_t = \frac{3}{2}p.\left(\Psi_d.I_q - \Psi_d.I_d\right) \qquad (106)$$

Harmonics originate exclusively from the grid-side inverter. Their frequencies are contingent upon the switching frequency (about voltage harmonics) and the inverter's pulse number (associated with current harmonics). The magnitude is dictated by the pulse duty factor, DP [52].

$$DP = \frac{n_{on}}{n_{on} + n_{off}} \qquad (107)$$

The effective impedance, which includes both the inverter and grid impedance, determines the presence of interharmonics. Interharmonics are generated solely when there are variations in the pulse duty factor due to fluctuations in the load. This occurrence is routine in the operation of WECs due to their variable-speed characteristics. Table 3 summarizes the SG specifications used in the simulation studies.

TABLE 2. DFIG specifications/parameters with units.

RATED STATOR VOLTAGE	480 (V$_{RMS}$)
RATED STATOR CURRENT	331A
RATED POWER P$_N$	275 KVA
RATED SPEED	1000 RPM
RATED FREQUENCY F	50Hz
STATOR RESISTANCE R$_s$	1.33 P.U
MUTUAL INDUCTANCE LM	3.5(P.U)
STATOR INDUCTANCE L$_S$	0.06(P.U)
ROTOR INDUCTANCE L$_R$	0.06(P.U)
NUMBER OF POLES P	4 POLE PAIRS
LUMPED INERTIA CONSTANT	2 H(S)
FREQUENCY MODULATION	1000 Hz

V. RESULTS AND DISCUSSIONS

The incremental GAN model is used to analyze the variations in wind conditions, and its effectiveness is compared to that of alternative approaches.

A. SIMULATION SETUP

The incremental GAN model has been deployed and tested using MATLAB, specifically in the 2022b version, on a Windows 10 platform equipped with 8GB of RAM. The primary objective behind this setup is to thoroughly assess the model's performance and gauge its progress and improvements in functionality and results with 10 m/s.

B. PERFORMANCE ANALYSIS BASED ON TIME

The authors presented a comprehensive overview of the performance metrics for the incremental GAN models applied to the analysis of variations in wind conditions from Fig. 7 to Fig. 14.

Figure 7: The incremental GAN approach consistently demonstrates remarkable performance, achieving frequency values of 50.075Hz, 50.118 Hz, 50.201 Hz, 50.272 Hz, and 50.285 Hz across epochs 10, 20, 30, 40, and 50, all within a time frame of 0.06*11 = 0.66 seconds. The Epoch 10/20/30/40/50 series of events pertains to, a total = 60 seconds, and time interval = 60 / 1000 = 0.06 seconds (or 60 milliseconds), 0.06*2 = 0.12. This calculation correctly converts the time from seconds to milliseconds. The training stages of a machine learning model, showcasing its performance at different training iterations.

On the other hand, variations in droop values are associated with control systems, representing changes in voltage or frequency levels to maintain stability in electrical systems.

Figure 8: In this subfigure, the incremental GAN strategy showcases its ability to maintain steady main load (kW) values, recording 53.28 kW, 53.40 kW, 53.41 kW, 53.42 kW, and 53.63 kW while adhering to the 0.12 seconds time frame. The main load refers to the total electrical demand from various devices and systems in a power network. It encompasses residential, commercial, or industrial loads and represents overall power consumption. It is distinct from the "DFIG rating," which specifically relates to the capacity of a DFIG used in wind turbines. The DFIG rating is a characteristic of the generator, while the main load is the electrical demand

TABLE 3. SG specifications/parameters with units.

NOMINAL POWER (P_N)	300 KVAR
LINE-TO-LINE VOLTAGE (V_N)	480 (V_{RMS})
RATED FREQUENCY	50 HZ
D AXIS RESISTANCE R_D	2.24 (p.u.)
Q AXIS RESISTANCE R_1	1.02 (p.u.)
D AXIS REACTANCE X_S	0.17 (p.u.)
Q AXIS REACTANCE X_Q	0.12 (p.u.)
STATOR RESISTANCE	0.017
INERTIA CONSTANT	1H(s)
POLE PAIRS	2 POLE PAIRS

or consumption that the generator is designed to serve. The DFIG must be appropriately sized to meet the requirements of the main load.

Figure 9: The incremental GAN strategy further demonstrates its effectiveness by consistently producing secondary load (kW) values of 156.65 kW, 157.01 kW, 157.02 kW, 157.04 kW, and 157.68 kW throughout the analysis, maintaining the time frame at 0.12 seconds. Secondary load likely refers to the electrical load demand that is not considered the primary load in the system. The mentioned values 156.65 kW and 157.68 kW for the secondary load, are likely measurements of power consumption. These values represent the electrical load in kW at various points in the analysis. It's important to note that secondary load is not typically used to describe a system rating. Instead, it refers to the actual power demand or consumption in the system at specific times during the analysis.

Figure 10: This subfigure provides insight into the speed performance of the incremental GAN approach. It achieves impressive speed values of 1263.63 rpm, 1263.68 rpm, 1264.26 rpm, 1264.36 rpm, and 1263.45 rpm across various epochs, all while maintaining a consistent 0.12-second interval. The x-difference of the graph indicates the time in seconds and the y-difference indicates the speed in rpm.

Figure 11: Continuing the analysis, the incremental GAN strategy reveals its capabilities in managing sync condenser values. These values consistently show results of 27.33 kvar, 30.03 kvar, 30.16 kvar, 30.33 kvar, and 45.71 kvar within the same 0.12-second time frame. The x-difference of the graph indicates the time in seconds and the y-difference indicates the sync condenser in kvar.

Figure 12: Fig. 12 provides insights into the power performance of the incremental GAN approach, which is the DFIG power. It achieves active power levels of 206.75 kW, 207.87 kW, 207.94 kW, 208.07 kW, and 209.57 kW across different epochs, all while maintaining the consistent 0.12-second analysis period. The x-difference of the graph indicates the time in seconds and the y-difference indicates the wind turbine power in kW.

Figure 13: The provided reactive power values for the wind turbine DFIG component in the incremental GAN approach appear to be very close, with slight variations across different epochs. All three components achieve voltage levels of 231.63 kvar, 231.66 kvar, 231.67 kvar, 231.78 kvar, 231.806 kvar. These voltage levels are
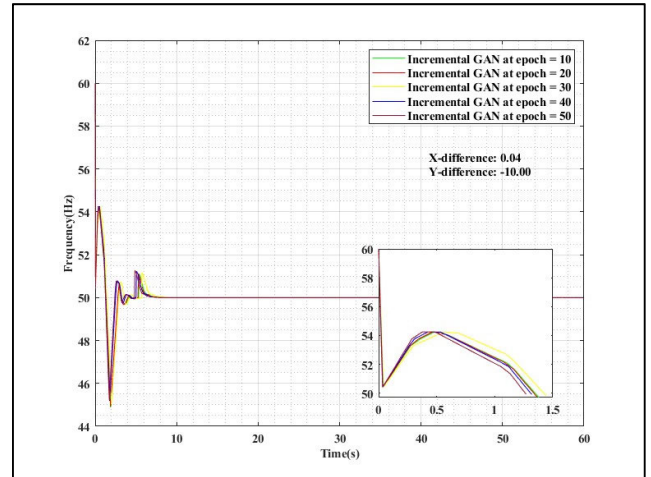
FIGURE 7. The incremental GAN approach, achieving frequency (Hz) response.
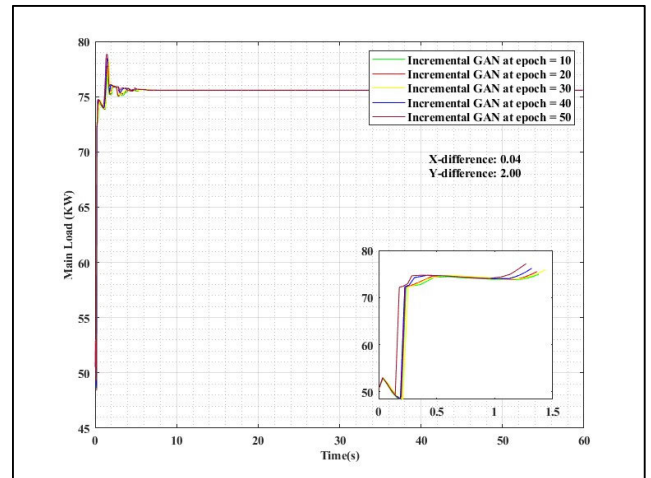

FIGURE 8. The incremental GAN approach, achieving main load (kW) response.

maintained consistently throughout the 0.12-second analysis period. The x-difference of the graph indicates the time in seconds and the y-difference indicates the wind turbine voltage in kvar.

Figure 14: The torque produced by the incremental GAN approach appears to be very close, with slight variations across different epochs ranging from 10-50. The values obtained at different epochs of 10-50 are 98.02 (N-m), 98.97 (N-m), 100.16 (N-m), 100.45 (N-m), and 101.12 (N-m) respectively. The x-difference of the graph indicates the time in seconds and the y-difference indicates the torque in N-m. These results collectively illustrate the robustness and stability of the incremental GAN models in handling various performance metrics across different epochs and time intervals during the analysis of wind condition variations.
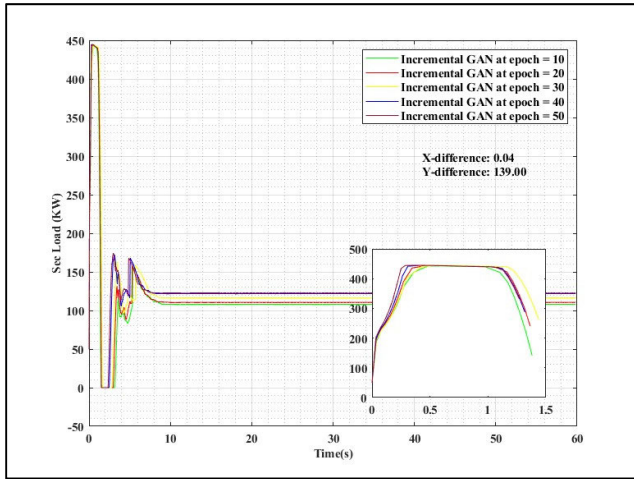
These results collectively illustrate the robustness and stability of the incremental GAN models in handling various performance metrics across different epochs and time intervals during the analysis of wind condition variations.

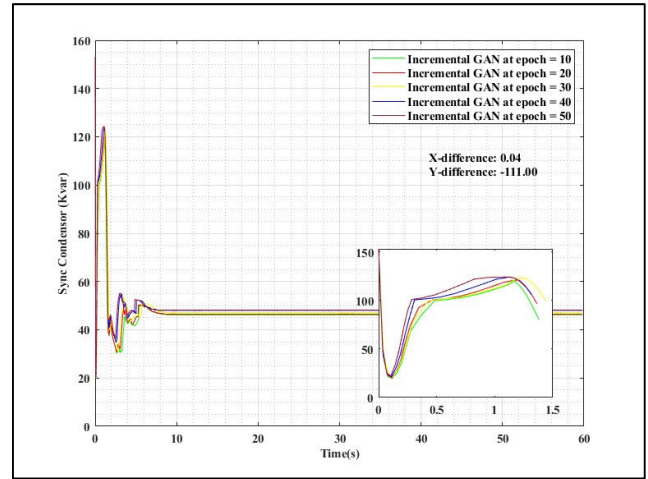FIGURE 9. The incremental GAN approach, achieving secondary load (kW) response.

FIGURE 10. The incremental GAN approach, achieving speed (rpm) response.

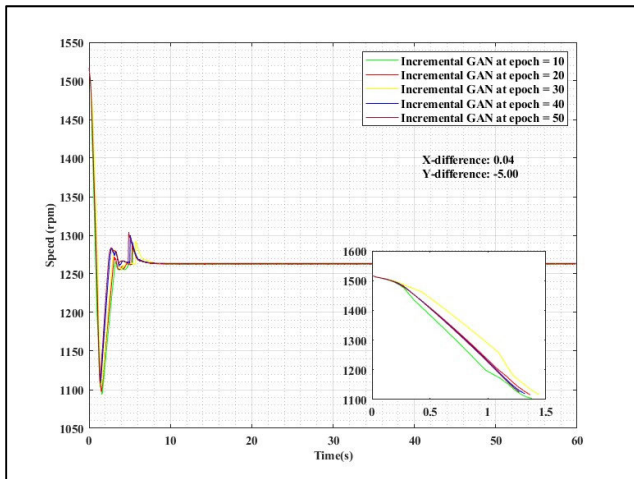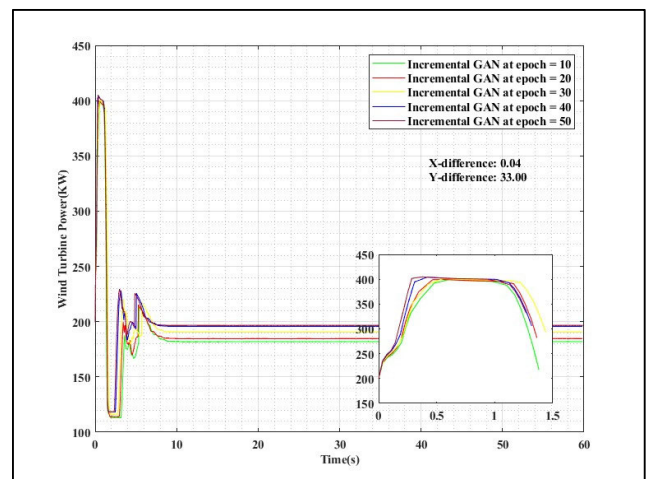FIGURE 11. The incremental GAN approach, achieving sync condenser (kvar) response.

FIGURE 12. The incremental GAN approach, wind turbine active power (kW) response.

C. SIMULATION RESULTS COMPARISON OF DIVERSE TECHNIQUES INCLUDING ANN, FOPI, FUZZY, CNN, AND THE PROPOSED IGAN

A rigorous comparative analysis was meticulously carried out to gauge the effectiveness of the incremental GAN model when applied to the intricate task of analyzing wind condition variations. This evaluative process encompassed an exhaustive exploration of an array of diverse techniques and models, including ANN [54], fractional-order PI controllers [54], fuzzy-based robust control systems [55], deep CNN [55], and GAN [56]. Each of these approaches was thoughtfully introduced and meticulously studied within the confines of this research.

1) COMPARATIVE ANALYSIS BASED ON TIME

Figure 15 (Frequency): Fig. 15 provides a detailed insight into the frequency achieved by the incremental GAN model during the analysis of wind condition variations while consistently maintaining a time interval of 0.12 seconds. The time interval of 0.12 seconds likely represents the duration

over which the incremental GAN model's performance is evaluated in the context of wind condition variations.

Impressively, the incremental GAN model outshines the standard GAN model by a remarkable margin of 0.00027%, attaining a frequency of 50.0747 Hz. This notable improvement underscores the model's superior performance in accurately predicting and stabilizing frequency.

Figure 16 (Main Load): Moving to Fig. 16, examine the steady main load in the context of wind condition analysis, with the incremental GAN model maintaining the same 0.12 second time interval. Demonstrating its superiority over the conventional GAN model, the incremental GAN model achieves an outstanding steady main load of 53.63 kW, surpassing its counterpart by a significant margin of 0.04%.

This achievement underscores the model's ability to maintain a consistent and efficient main load.

Figure 17 (Secondary Load): Fig. 17 focuses on the secondary load achieved by the incremental GAN model during wind condition analysis, with the time interval held at 0.12 seconds. Notably, the incremental GAN model surpasses
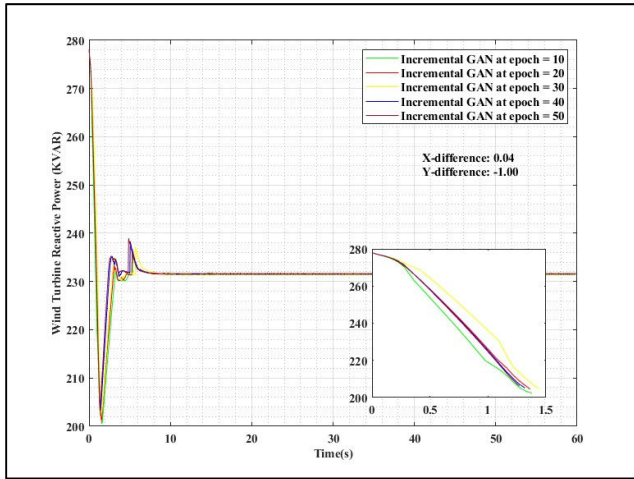
FIGURE 13. The incremental GAN approach, wind turbine reactive power (kvar) response.
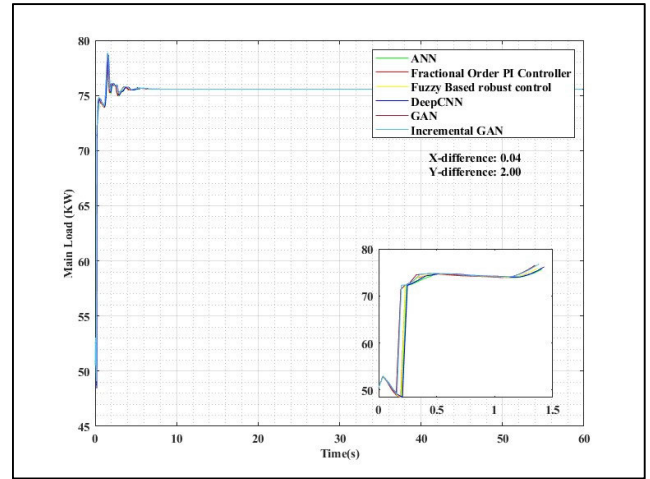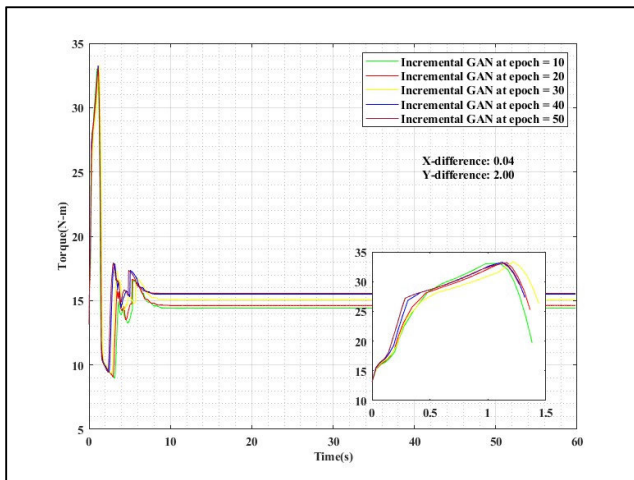

FIGURE 14. The incremental GAN approach, wind turbine Torque (N-m) response.

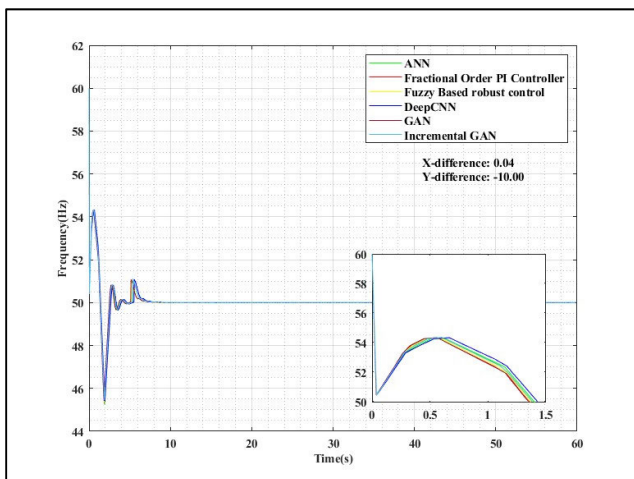**FIGURE 15.** Comparative frequency (Hz) analysis based on Time.

FIGURE 16. Comparative main load (kW) analysis based on Time.

FIGURE 17. Comparative secondary load (kW) analysis based on Time.

Figure 18 (Speed): In Fig. 18, the authors delve into the speed achieved by the incremental GAN model for the analysis of wind condition variations, maintaining the consistent 0.12-second time frame. Impressively, the incremental GAN model outperforms the GAN model by a significant margin of 0.0689%, reaching an impressive speed of 1261.03 rpm. This achievement reflects the model's superior ability to respond to changes in wind conditions.

Figure 19 (Sync Condenser): Fig. 19 illustrates the sync condenser achieved by the incremental GAN model during the analysis of wind conditions while adhering to a 0.12-second time frame. Remarkably, the incremental GAN model outperforms the GAN model by an impressive margin of 6.86%, achieving a sync condenser of 45.71 kvar. This substantial improvement underscores the model's effectiveness in managing synchronization condenser values.

Figure 20 (DFIG active power): Fig. 20, explores the wind turbine power achieved by the incremental GAN model for the analysis of wind condition variations, maintaining the same 0.12-second time interval. Impressively, the incremental GAN model outperforms the GAN model by a significant margin of 0.3183%, reaching a power output of 212.90 kW.
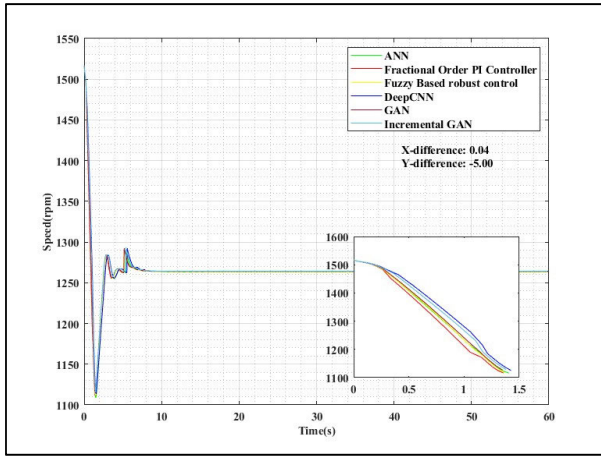
the secondary load of the GAN model by an impressive 0.04%, achieving a secondary load of 157.68 kW. This result highlights the model's capacity to handle secondary load fluctuations effectively.

FIGURE 18. Comparative speed (p.u.) analysis based on Time.
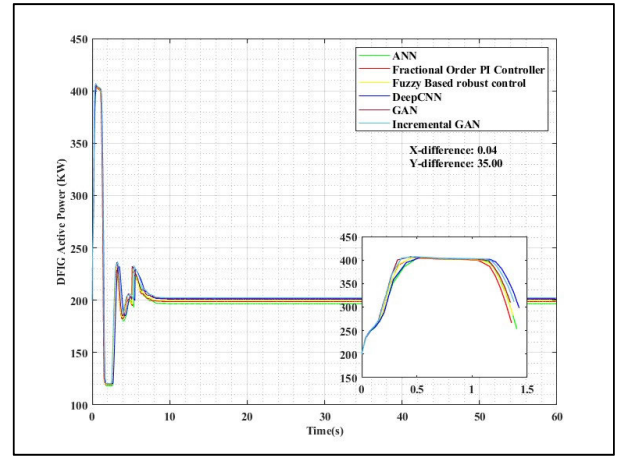

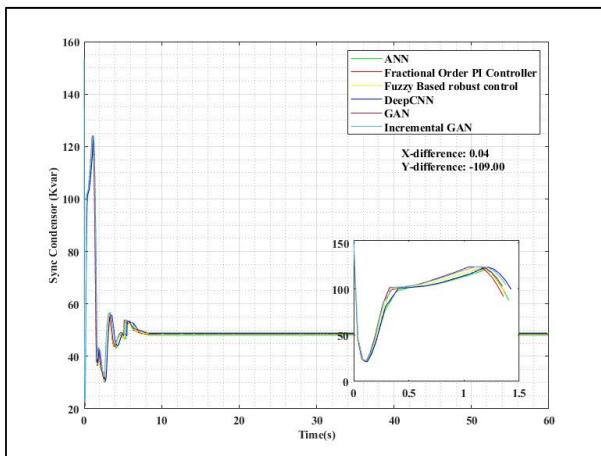**FIGURE 20.** Comparative DFIG Active Power (kW) analysis based on Time.

FIGURE 19. Comparative synchronous condenser (kvar) analysis based on Time.
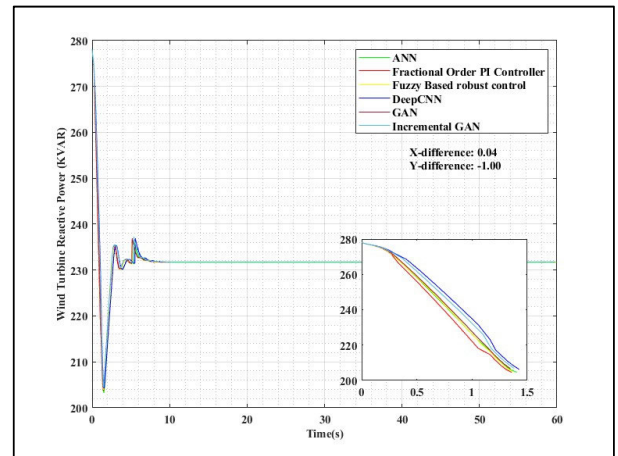

FIGURE 21. Comparative DFIG Reactive Power (kvar) analysis based on Time.

This result highlights the model's enhanced efficiency in harnessing wind energy and converting it into usable power. The x-difference of the graph represents the time in seconds and y-difference represents power in kW.

Figure 21 (DFIG Reactive power): Fig. 21, explores the wind turbine reactive power achieved by the incremental GAN model for the analysis of wind condition variations, maintaining the same 0.12-second time interval. Impressively, the incremental GAN model outperforms the GAN model by a significant margin of 0.06892%, reaching a power output of 271 kvar. This result highlights the model's enhanced efficiency in harnessing wind energy and converting it into usable power. The x-difference of the graph indicates the time in seconds and the y-difference indicates the wind turbine power in kvar.

Figure 22 (DFIG voltage): Fig. 22, explores the DFIG system voltage achieved by the incremental GAN model for the analysis of wind condition variations, maintaining the same 0.12 second time interval. Impressively, the incremental GAN model outperforms the GAN model by a significant margin of 0.0018%, reaching a DFIG system voltage of 1.00829 p.u. This result highlights the model's enhanced efficiency in harnessing wind energy and converting it into usable power.
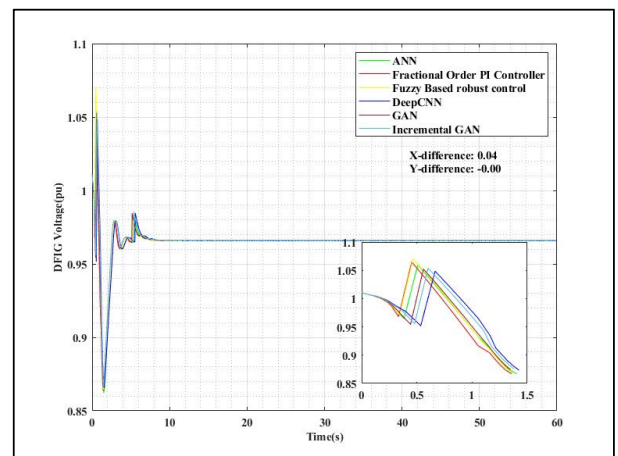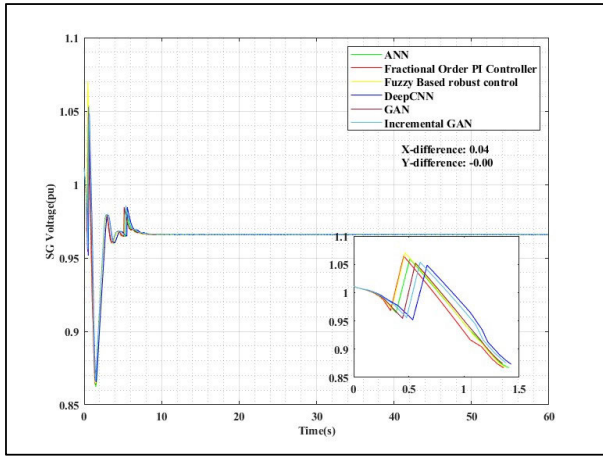

FIGURE 22. Comparative DFIG voltage (p.u.) analysis based on Time.

The x-difference of the graph indicates the time in seconds and the y-difference indicates the DFIG voltage in p.u.

Figure 23 (SG voltage): Fig. 23, explores the SG voltage achieved by the incremental GAN model for the analysis of wind condition variations, maintaining the same 0.12-second time interval. Impressively, the incremental GAN model outperforms the GAN model by a significant margin of

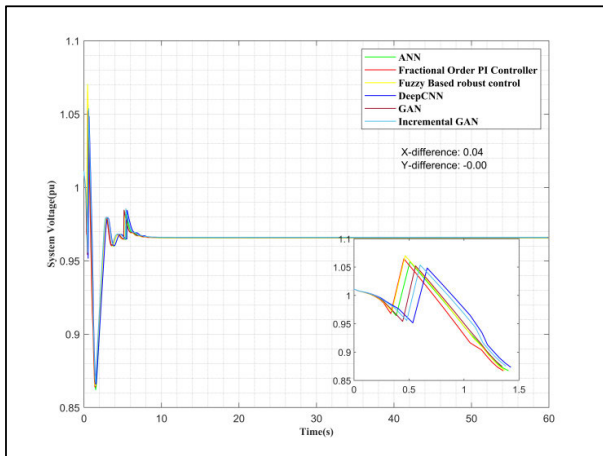**FIGURE 23.** Comparative SG voltage (p.u.) analysis based on Time.

FIGURE 24. Comparative System voltage (p.u.) analysis based on the Time.

TABLE 4. A comparative discussion in analyzing wind speed direction involves evaluating different methods and techniques used to assess wind direction data.

METHODS	FREQUENCY	MAIN LOAD	SEC LOAD	SPEED	SG kvar	WIND TURBINE POWER
ANN	50.0710	53.40	156.92	1.0108	29.17	209.57
FOPI	50.0723	53.51	157.00	1.0108	29.66	209.98
FUZZY BASED ROBUST CONTROL	50.0740	53.58	157.32	1.0109	33.62	210.03
DEEP CNN	50.0741	53.61	157.54	1.0109	40.23	212.22
GAN	50.0746	53.63	157.61	1.0110	42.57	212.22
PROPOSED INCREMENTAL GAN	50.0747	53.38	157.68	1.0110	45.71	212.90

Note: The column header "TIME FRAME" spans the columns FREQUENCY, MAIN LOAD, SEC LOAD, SPEED, SG kvar, WIND TURBINE POWER.

0.002 reaching an SG voltage of 1.0084 p.u. The x-difference of the graph indicates the time in seconds and the y-difference indicates the SG voltage in p.u.

Figure 24 (system voltage): Fig. 24, explores the system voltage achieved by the incremental GAN model for the analysis of voltage variations, maintaining the same 0.12 second time interval. Impressively, the incremental GAN model outperforms the GAN model by a significant margin of 0.002 reaching a system voltage of 0.0064 p.u. The x-difference of the graph indicates the time in seconds and the y-difference indicates the system voltage in p.u.

2) COMPARATIVE DISCUSSIONS

Table 4 summarizes a comparative discussion in analyzing wind speed direction involves evaluating different methods and techniques used to assess wind direction data. It involves an in-depth exploration of each approach's strengths, weaknesses, performance, and applicability in the context of analyzing wind condition variations. Ultimately, this enhanced performance could lead to increased energy production, reduced operational costs, or more reliable power generation, making the proposed model a preferred choice for wind turbine analysis applications. Here a reduction in the

main load and an increase in the secondary load can benefit the system, it can indeed be advantageous in certain situations. By reducing the main load to a range of 0-50 kW and simultaneously increasing the secondary load to a range of 0-450 kW, a more balanced load distribution is achieved. This balance can lead to improved overall system performance. With a reduced main load, there's a lower risk of overloading primary components, and the increased secondary load helps utilize available capacity efficiently. This approach can enhance system stability, minimize energy waste, and lead to better resource utilization, contributing to enhanced system efficiency and reliability. However, the specific benefits depend on the system's characteristics and requirements.

VI. CONCLUSION

In conclusion, this research represents a significant step forward in the field of wind energy generation, its integration into the power grid, and power system stability management. Deploying the Incremental Tuned GAN and harnessing parameters including climate, load, wind speed, and wind penetration, have paved the way for enhanced efficiency and reliability in the utilization of wind energy resources. The incorporation of adaptive discriminators, self-attention mechanisms, and the generation of key parameters like droop gain and optimized gain parameters has substantially improved the accuracy of wind data predictions. Furthermore, our focus on grid stability, particularly in the context of DFIG and SG, underscores the importance of the seamless integration of renewable energy sources into existing power systems. This research's iterative approach, where the Incremental Tuned GAN continuously assesses and refines wind farm conditions, ensures that power generation remains responsive to changing circumstances. At 0.12 seconds of analysis time, the incremental GAN model achieves specific operational parameters, a frequency of 50.0747 Hz, a primary

load demand of 53.38 kW, a secondary load demand of 157.68 kW, a generator speed of 1.0110 per unit, a synchronous condenser rating of 45.71 kvar, and a wind turbine power output of 212.90 kW. In the future, the research will be extended to use a six-phase DFIG system to analyse the system performance.

A. CONTRIBUTION

- **Incremental Tuned GAN:** This research aims at the development and application of an incremental tuned GAN technique tailored for wind energy management. This incremental GAN methodology, powered by climate, load, wind speed, and wind penetration parameters, significantly enhances predictive accuracy through continuous training. It employs advanced discriminators and self-attention mechanisms to refine predictions and generates critical parameters for grid stability and optimized wind energy generation. In essence, the Incremental Tuned GAN serves as the research's core tool for achieving accurate, real-time wind data predictions, thus improving wind energy management.

- **Control strategies of Grid-Tied DFIG and SG:** The primary contribution of grid-integrated wind farms based on the DFIG and an independent SG in this research is to optimize their control strategies for better grid stability and reliability, particularly when incorporating wind energy. This ensures a smoother transition to cleaner energy sources and more efficient grid management, reducing disruptions caused by variable wind power. In essence, DFIGs and SGs' operational characteristic improvements enhance the integration of wind energy into the power grid, promoting sustainability and reliability.

REFERENCES

[1] International Energy Agency. (2022). *International Energy Agency (IEA) World Energy Outlook 2022.* [Online]. Available: https://Www.Iea.Org/Reports/World-Energy-Outlook-2022/Executive-Summary

[2] D. Byles and S. Mohagheghi, "Sustainable power grid expansion: Life cycle assessment, modeling approaches, challenges, and opportunities," *Sustainability*, vol. 15, no. 11, p. 8788, May 2023, doi: 10.3390/su15118788.

[3] N. Ullah, I. Sami, Md. S. Chowdhury, K. Techato, and H. I. Alkhammash, "Artificial intelligence integrated fractional order control of doubly fed induction generator-based wind energy system," *IEEE Access*, vol. 9, pp. 5734–5748, 2021, doi: 10.1109/ACCESS.2020.3048420.

[4] M. Debouza and A. Al-Durra, "Grid ancillary services from doubly fed induction generator-based wind energy conversion system: A review," *IEEE Access*, vol. 7, pp. 7067–7081, 2019, doi: 10.1109/ACCESS.2018.2890168.

[5] Z. Tir, O. P. Malik, and M. N. Hashemnia, "Intelligent control of a brushless doubly-fed induction generator," *Int. J. Syst. Assurance Eng. Manage.*, vol. 10, no. 3, pp. 326–338, Jun. 2019, doi: 10.1007/s13198-019-00772-2.

[6] I. Yaichi, A. Semmah, and P. Wira, "Control of doubly fed induction generator with maximum power point tracking for variable speed wind energy conversion systems," *Periodica Polytechnica Electr. Eng. Comput. Sci.*, vol. 64, no. 1, pp. 87–96, Nov. 2019, doi: 10.3311/ppee.14166.

[7] India Energy Outlook. (2021). *India Energy Outlook 2021—Analysis IEA.* India Energy Outlook. [Online]. Available: www.iea.org/weo

[8] P. Ponce, J. A. Rosales, A. Molina, H. Ponce, and B. MacCleery, "Designing a robust controller using SMC and fuzzy artificial organic networks for brushed DC motors," *Energies*, vol. 13, no. 12, p. 3091, Jun. 2020, doi: 10.3390/en13123091.

[9] C. Mukonza and G. Nhamo, "Wind energy in South Africa: A review of policies, institutions and programmes," *J. Energy Southern Afr.*, vol. 29, no. 2, pp. 21–28, Jun. 2018.

[10] A. R. Nejad, "Wind turbine drivetrains: State-of-the-art technologies and future development trends," *Wind Energy Sci.*, vol. 7, no. 1, pp. 387–411, Feb. 2022, doi: 10.5194/wes-7-387-2022.

[11] *WIND FORCE 12 A Blueprint to Achieve 12% of the World's Electricity From Wind Power by 2020*, Wind Force, European Wind Energy Association and Greenpeace, Colombo, Sri Lanka, Jun. 2005, pp. 1–52.

[12] J. F. Manwell, J. G. McGowan, and A. L. Rogers, *Wind Energy Explained Theory, Design, and Applications*. U.K.: Wiley, 2009. [Online]. Available: https://ee.tlu.edu.vn/Portals/0/2018/NLG/Sach_Tieng_Anh.pdf

[13] A. Hemami, *Wind Turbine Technology*. Boston, MA, USA: Cengage Learning, 2012, doi: 12345XX111009.

[14] M. Juraeva, J.-H. Lee, and D.-J. Song, "A computational analysis of the train-wind to identify the best position for the air-curtain installation," *J. Wind Eng. Ind. Aerodynamics*, vol. 99, no. 5, pp. 554–559, May 2011, doi: 10.1016/j.jweia.2011.02.004.

[15] H. Jing, H. Liao, C. Ma, Q. Tao, and J. Jiang, "Field measurement study of wind characteristics at different measuring positions in a mountainous valley," *Experim. Thermal Fluid Sci.*, vol. 112, Apr. 2020, Art. no. 109991, doi: 10.1016/j.expthermflusci.2019.109991.

[16] R. Akbari, A. Izadian, and R. S. Weissbach, "Quasi self-excited DFIG-based wind energy conversion system," *IEEE Trans. Ind. Appl.*, vol. 57, no. 3, pp. 2816–2824, May 2021, doi: 10.1109/TIA.2021.3067621.

[17] I. Angulo, D. de la Vega, I. Cascón, J. Cañizo, Y. Wu, D. Guerra, and P. Angueira, "Impact analysis of wind farms on telecommunication services," *Renew. Sustain. Energy Rev.*, vol. 32, pp. 84–99, Apr. 2014, doi: 10.1016/j.rser.2013.12.055.

[18] N. Naeeni and M. Yaghoubi, "Analysis of wind flow around a parabolic collector (1) fluid flow," *Renew. Energy*, vol. 32, no. 11, pp. 1898–1916, Sep. 2007, doi: 10.1016/j.renene.2006.10.004.

[19] X. Chen and J. Z. Xu, "Structural failure analysis of wind turbines impacted by super typhoon usagi," *Eng. Failure Anal.*, vol. 60, pp. 391–404, Feb. 2016, doi: 10.1016/j.engfailanal.2015.11.028.

[20] B. C. Babu and K. B. Mohanty, "Doubly-fed induction generator for variable speed wind energy conversion systems-modeling & simulation," *Int. J. Comput. Electr. Eng.*, vol. 2, pp. 141–147, Jun. 2010, doi: 10.7763/ijcee.2010.v2.127.

[21] X. Zhao, Z. Lin, B. Fu, and S. Gong, "Research on frequency control method for micro-grid with a hybrid approach of FFR-OPPT and pitch angle of wind turbine," *Int. J. Electr. Power Energy Syst.*, vol. 127, May 2021, Art. no. 106670, doi: 10.1016/j.ijepes.2020.106670.

[22] C. Wei, M. Han, S. Lin, and X. Li, "Low voltage ride-through control strategy of a large capacity DFIG with grid-side thyristor controlled voltage regulator," in *Proc. IET Conf. Renew. Power Gener. (RPG)*, Sep. 2011, pp. 1–6, doi: 10.1049/cp.2011.0215.

[23] B. Lu, S. Li, H. S. Das, Y. Gao, J. Wang, and M. Baggu, "Dynamic P-Q capability and abnormal operation analysis of a wind turbine with doubly fed induction generator," *IEEE J. Emerg. Sel. Topics Power Electron.*, vol. 10, no. 4, pp. 4854–4864, Aug. 2022, doi: 10.1109/JESTPE.2021.3133527.

[24] E. Haile, G. Worku, A. M. Beyene, and M. Tuka, "Modeling of doubly fed induction generator based wind energy conversion system and speed controller," *J. Energy Syst.*, vol. 5, no. 1, pp. 46–59, Mar. 2021, doi: 10.30521/jes.854669.

[25] J. D. A. de Oliveira, F. K. D. A. Lima, F. L. Tofoli, and C. G. C. Branco, "Synchronverter-based frequency control technique applied in wind energy conversion systems based on the doubly-fed induction generator," *Electric Power Syst. Res.*, vol. 214, Jan. 2023, Art. no. 108820, doi: 10.1016/j.epsr.2022.108820.

[26] R. K. Behara and A. K. Saha, "Artificial intelligence control system applied in smart grid integrated doubly fed induction generator-based wind turbine: A review," *Energies*, vol. 15, no. 17, p. 6488, Sep. 2022, doi: 10.3390/en15176488.

[27] L. A. G. Gomez, A. P. Grilo, M. B. C. Salles, and A. J. Sguarezi Filho, "Combined control of DFIG-based wind turbine and battery energy storage system for frequency response in microgrids," *Energies*, vol. 13, no. 4, p. 894, Feb. 2020, doi: 10.3390/en13040894.

[28] T.-H. Chien, Y.-C. Huang, and Y.-Y. Hsu, "Neural network-based supplementary frequency controller for a DFIG wind farm," *Energies*, vol. 13, no. 20, p. 5320, Oct. 2020, doi: 10.3390/en13205320.

[29] Z. Xiaoxun, X. Zixu, W. Yu, G. Xiaoxia, H. Hinyu, L. Hongkun, L. Ruizhang, C. Yao, and L. Huaxin, "Research on wind speed behavior prediction method based on multi-feature and multi-scale integrated learning," *Energy*, vol. 263, Jan. 2023, Art. no. 125593, doi: 10.1016/j.energy.2022.125593.

[30] T. Kobayashi, M. Sandberg, T. Fujita, E. Lim, and N. Umemiya, "Numerical analysis of wind-induced natural ventilation for an isolated cubic room with two openings under small mean wind pressure difference," *Building Environ.*, vol. 226, Dec. 2022, Art. no. 109694, doi: 10.1016/j.buildenv.2022.109694.

[31] Y. Guo, H. Gao, Q. Wu, J. Østergaard, D. Yu, and M. Shahidehpour, "Distributed coordinated active and reactive power control of wind farms based on model predictive control," *Int. J. Electr. Power Energy Syst.*, vol. 104, pp. 78–88, Jan. 2019, doi: 10.1016/j.ijepes.2018.06.043.

[32] T. Ilakkia and G. Vijayagowri, "Hybrid PV/wind system for reduction of harmonics using artificial intelligence technique," in *Proc. IEEE-Int. Conf. Adv. Eng., Sci. Manage. (ICAESM)*, Mar. 2012, pp. 303–308.

[33] H. Ali, G. Magdy, B. Li, G. Shabib, A. A. Elbaset, D. Xu, and Y. Mitani, "A new frequency control strategy in an islanded microgrid using virtual inertia control-based coefficient diagram method," *IEEE Access*, vol. 7, pp. 16979–16990, 2019, doi: 10.1109/ACCESS.2019.2894840.

[34] H. Benbouhenni and N. Bizon, "Improved rotor flux and torque control based on the third-order sliding mode scheme applied to the asynchronous generator for the single-rotor wind turbine," *Mathematics*, vol. 9, no. 18, p. 2297, Sep. 2021, doi: 10.3390/math9182297.

[35] Y. Chongjarearn and P. Laohachai, "Stator-voltage vector control of a doubly-fed induction generator," in *Proc. 34th Elect. Eng. Conf. (EECON-34)*, Chon Buri, Thailand, Nov. 2011, pp. 1–4.

[36] A. K. Agrawal, B. Munshi, and S. Kayal, "Study of wind turbine driven dfig using Ac/Dc/Ac converter," Tech. Rep., 2006.

[37] V. M. Gopala and Y. P. Obulesu, "A new hybrid artificial neural network based control of doubly fed induction generator," *Int. J. Electr. Comput. Eng. (IJECE)*, vol. 5, no. 3, p. 379, Jun. 2015, doi: 10.11591/ijece.v5i3.pp379-390.

[38] G. Tapia, A. Tapia, and J. X. Ostolaza, "Proportional–integral regulator-based approach to wind farm reactive power management for secondary voltage control," *IEEE Trans. Energy Convers.*, vol. 22, no. 2, pp. 488–498, Jun. 2007, doi: 10.1109/TEC.2005.858058.

[39] B. Desalegn, D. Gebeyehu, and B. Tamrat, "Evaluating the performances of PI controller (2DOF) under linear and nonlinear operations of DFIG-based WECS: A simulation study," *Heliyon*, vol. 8, no. 12, Dec. 2022, Art. no. e11912, doi: 10.1016/j.heliyon.2022.e11912.

[40] J. L. Rodriguez-Amenedo, S. Arnalte, and J. C. Burgos, "Automatic generation control of a wind farm with variable speed wind turbines," *IEEE Trans. Energy Convers.*, vol. 17, no. 2, pp. 279–284, Jun. 2002, doi: 10.1109/TEC.2002.1009481.

[41] C. B. Moorthy and M. K. Deshmukh, "Wind resource assessment using computer simulation tool: A case study," *Energy Proc.*, vol. 100, pp. 141–148, Nov. 2016, doi: 10.1016/j.egypro.2016.10.156.

[42] L. Tenghiri, Y. Khalil, F. Abdi, and A. Bentamy, "Optimum design of a small wind turbine blade for maximum power production," *IOP Conf. Ser. Earth Environ. Sci.*, vol. 161, no. 1, 2018, Art. no. 012008, doi: 10.1088/1755-1315/161/1/012008.

[43] M. Ragheb and A. M. Ragheb, "Wind turbines theory—The Betz equation and optimal rotor tip speed ratio," *Intechopen*, vol. 1, no. 1, pp. 1–22, 2011.

[44] P. Deka, "Influence of design parameters on the performance of Savonius wind turbine," *Artic. Int. J. Innov. Sci. Technol.*, vol. 7, no. 4, pp. 121–130, 2022. [Online]. Available: www.ijisrt.com

[45] J. N. Libii, "Comparing the calculated coefficients of performance of a class of wind turbines that produce power between 330 kw and 7,500 kw," *World Trans. Eng. Technol. Educ.*, vol. 11, no. 1, pp. 36–40, 2013.

[46] T. Ackermann, *Wind Power in Power Systems*. Hoboken, NJ, USA: Wiley, 2005.

[47] C. Hamon, K. Elkington, and M. Ghandhari, "Doubly-fed induction generator modeling and control in DigSilent PowerFactory," in *Proc. Int. Conf. Power Syst. Technol.*, Oct. 2010, pp. 1–7, doi: 10.1109/POWERCON.2010.5666596.

[48] M. Badreldien, R. Usama, A. El-wakeel, and A. Y. Abdelaziz, "Modeling, analysis and control of doubly fed induction generators for wind turbines," in *Proc. ICEENG Conf. ICEENG*, 2014, pp. 1–18, doi: 10.21608/iceeng.2014.30383.

[49] N. K. Mishra, Z. Husain, and A. Iqbal, "Modeling and analysis of novel six-phase DFIG through asymmetrical winding structure for disperse generation," *Int. Trans. Electr. Energy Syst.*, vol. 30, no. 12, Dec. 2020, Art. no. e12649, doi: 10.1002/2050-7038.12649.

[50] C. Chellaswamy, T. S. Geetha, P. Thiruvalar Selvan, and A. Arunkumar, "6-phase DFIG for wind energy conversion system: A hybrid approach," *Sustain. Energy Technol. Assessments*, vol. 53, Oct. 2022, Art. no. 102497, doi: 10.1016/j.seta.2022.102497.

[51] M. S. Marhaba, S. Farhangi, H. Iman-Eini, and R. Iravani, "Reactive power sharing improvement of droop-controlled DFIG wind turbines in a microgrid," *IET Gener., Transmiss. Distrib.*, vol. 12, no. 4, pp. 842–849, Feb. 2018, doi: 10.1049/iet-gtd.2016.2086.

[52] D. Schulz, R. Hanitsch, T. Kompa, and A. Samour, "Comparative power quality investigations of variable speed wind energy converters with doubly-fed induction and synchronous generator," in *Proc. Power Quality Conf.*, D. Schulz, R. Hanitsch, T. Kompa, A. Samour, Eds., Aug. 2015, pp. 39–44.

[53] I. A. Ahmed and A. F. Zobaa, "Comparative power quality study of variable speed wind turbines," *Int. J. Energy Convers. (IRECON)*, vol. 4, no. 4, p. 97, Jul. 2016, doi: 10.15866/irecon.v4i4.10828.

[54] S. Agatonovic-Kustrin and R. Beresford, "Basic concepts of artificial neural network (ANN) modeling and its application in pharmaceutical research," *J. Pharmaceutical Biomed. Anal.*, vol. 22, no. 5, pp. 717–727, Jun. 2000, doi: 10.1016/s0731-7085(99)00272-1.

[55] M. Dawei, Z. Yu, Z. Meilan, and N. Risha, "Intelligent fuzzy energy management research for a uniaxial parallel hybrid electric vehicle," *Comput. Electr. Eng.*, vol. 58, pp. 447–464, Feb. 2017, doi: 10.1016/j.compeleceng.2016.03.014.

[56] S. Soua, P. Van Lieshout, A. Perera, T.-H. Gan, and B. Bridge, "Determination of the combined vibrational and acoustic emission signature of a wind turbine gearbox and generator shaft in service as a pre-requisite for effective condition monitoring," *Renew. Energy*, vol. 51, pp. 175–181, Mar. 2013, doi: 10.1016/j.renene.2012.07.004.

RAMESH KUMAR BEHARA is currently pursuing the Ph.D. degree in electrical power engineering with the School of Engineering, University of KwaZulu-Natal, Durban, South Africa. He is also an Electrical Engineer with Mondi Papers. His research interests include advances in power systems and renewable energies control systems. He is also a registered Professional Engineering Technologist with the Engineering Council of South Africa and a member of SAIEE.

AKSHAY KUMAR SAHA (Senior Member, IEEE) is currently a Professor and an Academic Leader Research and Higher Degrees with the School of Engineering, University of KwaZulu-Natal, Durban, South Africa. His research interest includes advances of power systems in various areas, including engineering education. He has published more than 60 articles in top-tier international journals and over 100 international conference papers in relevant areas. He is also a registered Professional Engineer with the Engineering Council of South Africa and a fellow of the South African Institute of Electrical Engineers, South African Academy of Engineering. He is also a Senior Member of SAIMC, a member of Academy of Science of South Africa (ASSAf), and an Individual Member of Cigre. He was awarded the Best Lecturer Electrical Engineering, in 2013 and 2014, (2016–2019) by the School of Engineering, Research Excellence Award, in 2015 and 2022, and Top-30 Publishing Research Award for 2020 and 2021 by the University of KwaZulu-Natal. He is also acting as an editorial board member of a number of top-tier international journals. He is also a member of IEEE-HKN.

● ● ●